Addis Ababa University

Addis Ababa Institute of Technology

School of Civil and Environmental Engineering

STUDY ON FLEXURAL BUCKLING CURVES FOR HOT FINISHED HOLLOW SECTIONS

By

Temesgen Abiy

Advisor: **Dr. Shifferaw Taye**

Sponsor: **Ethiopian Roads Authority (ERA)**

March 2018

A thesis submitted to the School of Graduate Studies of Addis Ababa University in partial fulfillment of the requirements for the degree of Master of Science in Structural Engineering

The undersigned have examined the thesis entitled 'Study on Flexural Buckling Curves for Hot Finished Hollow Sections' presented by **Temesgen Abiy**, a candidate for the degree of **Master of Science** and hereby certify that it is worthy of acceptance.

Dr. Shifferaw Taye		
Advisor	Signature	Date
Dr. Bedilu Habte		
Internal Examiner	Signature	Date
Dr. Asnake Adamu		
External Examiner	Signature	Date
Dr. Agizew Nigussie		
Chair person	Signature	Date

UNDERTAKING

I certify that research work titled “Study on Flexural Buckling Curves for Hot Finished Hollow Sections” is my own work. The work has not been presented elsewhere for assessment. Where material has been used from other sources it has been properly acknowledged/referred.

_____

Temesgen Abiy

March 2018

ACKNOWLEDGMENTS

First and foremost I would like to thank the Almighty God for his unending blessings**.**

I would like to express my sincere appreciation to my advisor Dr. Shifferaw Taye for the support, guidance, encouragement, and insights he provided me throughout the study.

My thanks also go to Ethiopian Road Authority, for being the sponsor for my M.Sc. study.

Finally, I would like to express my deepest appreciation to my family for their confidence in me and for the support, love, and understanding.

TABLE OF CONTENTS

LIST OF TABLES

LIST OF FIGURES

NOTATIONS

Abbreviations

EC3	Eurocode 3
EN	European Standard
FE	Finite Element
FEA	Finite Element Analyses
FEM	Finite Element Method
GNA	Geometrically Non-linear Analysis
GMNA	Geometrically and Materially Non-linear Analysis
GMNIA	Geometrically and Materially Non-linear Imperfect Analysis
HR	Hot-Rolled
LBA	Linear buckling analysis
MNA	Materially nonlinear analysis
RHS	Rectangular Hollow Section
SHS	Square Hollow Section

Symbols

A	Cross-sectional area of a steel column
A_{eff}	Effective area of a cross-section
B	width of a cross-section
e_0	Initial bow imperfection amplitude
E	Modulus of elasticity
f_y	Yielding strength
F_{max}	Maximum of axial compressive force applied on a steel column
H	Height of a cross-section
I	Radius of gyration of a cross section
i_y	Radius of gyration along major axis
i_z	Radius of gyration along minor axis
I	Second moment of area
I_y	Second moment of area with respect to major axis
I_z	Second moment of area with respect to minor axis
L	Length of a column
M(x)	Bending moment at x - position along the length of a column
M_{ed}	Design bending moment
M_e	External moment
M_i	Internal moment

N	Axial compressive load applied on a steel column.
$N_{b,Rd}$	Design buckling resistance of the compression member
N_{cr}	Elastic critical force for the relevant buckling mode
N_{Ed}	Design value of the compressive force
N_{Rd}	Design values of the resistance to normal forces
T	Thickness of the cross-section.
W_{el}	Elastic section modulus
X	Predefined position along a column length
Y	Deflection of a column at x - position along the length of a column
$y(0)$	Deflection at starting point of a column
$y(L)$	Deflection at the end of a column
α	Imperfection factor
γ_{M1}	Partial factor for member buckling resistance
ε_{true}	True strain
Φ	Intermediate factor
σ_{cr}	Critical elastic buckling stress
σ_{true}	True stress
$\overline{\lambda}$	Non-dimensional slenderness
λ	Geometric slenderness ratio of a column
χ	Reduction factor for relevant buckling mode

ABSTRACT

This work focuses mainly on the resistance of members to flexural buckling according to Eurocode 3. The work provides the mathematical backgrounds to the equations and buckling curves presented in Eurocode 3. The work also attempts to reveal how material behavior and residual stress influence the flexural buckling resistance which is demonstrated through finite element (FE) simulations.

The work presents modeling and analysis on hollow section columns in ABAQUS 6.14. Linear and non-linear buckling analyses of the hollow section columns, with the imperfections, are implemented in this work. Specifically, the imperfections considered in this study are material plasticity, initial bow and residual stress.

It was found that mesh size influences buckling behavior. Elastic-plastic with a strain hardening slope of E/100 gives a little higher buckling load but did not significantly affect the results. Residual stresses influence buckling behavior. Both material behavior and residual stresses influence reduce when the column heights increases. The rectangular section has high buckling curve than that of square section with same slenderness ratio. The minor axis have high buckling curve when the ratio of height to width(h/b) of cross sections high but the major axis buckling have the same buckling curves given in Eurocode 3.

Keywords: Finite element analyses, Buckling curves, Eurocode 3, Flexural buckling, Geometric imperfection, Linear-buckling analysis, Residual stress, Hollow sections.

CHAPTER 1 INTRODUCTION

1.1 Application of Tubular Sections

The use of hollow structural steel has been increasing in the past few years. Although the price per ton of hollow sections is much higher than that of open profiles, their aesthetic appeal and their enhanced static values allow lighter construction and economic structures. Long-span roof structures and industrial buildings are increasingly designed with structural hollow sections. Modern architecture is dominated by tubular cold-formed structure, while industrial structures are dominated by hot-rolled tubular sections. Figure 1-1 shows some astonishing tubular structures made around the world [1].

Figure 1-1: Australia stadium (Australia), Madrid Barajas international airport (Spain), London eye (Britain).

The increase use of tubular sections is not only due to their excellent architectural aspect but also to their economic advantages in comparison with open sections. Square, rectangular or round cross-sections have outstanding static properties which can be presented as follows [1]:

(i) Their excellent behavior towards global buckling, lateral torsional buckling and torsion is due to their closed shape and the favorable distribution of material around the longitudinal axis of the section;

(ii) The use of the internal volume to increase the load bearing capacity of the column by filling it with concrete;

(iii) The corrosion protection can be applied economically compared to open sections considering that hollow sections have smaller and smoother surfaces without any sharp edges.

However, the use of hollow sections presents an inconvenient for the case of elements for which bending is the primary action since the uniform distribution of material around the longitudinal axis of the section would constitute a handicap compared to open sections (H or I). Indeed, for bending, hollow profiles have generally a high sufficient thickness (due to both webs) to absorb shear stresses, but the flange thicknesses are not economically sufficient to absorb the normal stresses due to bending. Therefore, the hollow profiles are undeniably the ideal profiles for columns while open profiles are more suitable for the beams. However, the occurrence of lateral torsional buckling in open sections may change this last conclusion and make the hollow profiles best suited to be used for both columns and beams.

The buckling behavior of hollow profiles becomes even better when the material is distributed as far as possible from the longitudinal axis of the section. For an identical area, one comes to consider that economy will lead to hollow profiles of greater widths and smaller thicknesses. The resulting thinness of the plates may, however, lead to another phenomenon of instability named ‘local buckling’ which is not discussed in this thesis. To avoid local buckling all the column sections selected in this thesis fulfill minimum of class three according to European classification.

There are two types of steel hollow sections and they are distinguished by the method of production:

- cold formed hollow sections
- hot formed hollow profiles

Cold-formed hollow sections are formed in a process where most of the forming of the tube is performed at room temperature or ambient temperature, and the final product is delivered without additional heat treatment. (Welding and after treatment of seam are not considered as heat treatment). The way of production and supply is determined by the European standard EN 10219 [2]. Cold formed are welded structural sections of non-alloy and fine grain steels. The method of production of the hot-formed hollow section is quite different. This ultimately results in certain differences in tolerance, performance, and mechanical properties, in at first glance identical hollow profiles.

Hot formed hollow sections can be produced in two ways:

- hot forming - with or without additional heat treatment (seamless hollow sections)
- cold forming, with additional heat treatment (welded hollow sections which the removed seam)

They can be delivered in the normalized or normalized rolled state. Hot rolled hollow profiles produced by the method of heat treatment, where the final forming is performed at temperatures from 700 ° to 900 ° C, which is the range of normalization.

The standard EN 10210 [3, 4]- Hot finished seamless structural hollow sections of non-alloy and fine grain steels accurately determine the way of production, supply, labeling and permitted tolerance

EN 10210-1 [3] - defines the technical requirements for the delivery of round, square and rectangular cold formed hollow sections

EN 10210-2 [4] - specifies tolerances, dimensions and sectional properties

Standard EN 10210, among others determines unambiguous labeling of products

- for hot-formed non-alloy steel hollow sections the steel designation consists of
  - the number of European Standard – EN 10210
  - capital letter **S** for structural steel
  - indication that shows the required minimum yield strength for thickness ≤16 mm expressed in MPa
  - capital letters that indicate bending rupture that material can withstand
    - ✓ **JR** at room temperature
    - ✓ **J0** at temperature of 0°C

- ✓ **J2** and **K2** at temperature of -20°C
- capital letter **H** which indicates hollow sections

EXAMPLE Structural steel (S) with a specified minimum yield strength for a thickness not greater than 16 mm of 275 MPa, with a minimum impact energy value of 27 J at 0 °C (J0), hollow section (H): EN 10210-S275J0H

– for fine grain steel structural hollow sections the steel designation consists of
  - the number of European Standard – EN 10210
  - capital letter **S** for structural steel
  - indication that shows the required minimum yield strength for thickness ≤16 mm expressed in MPa
  - capital letter **N** to indicate normalized or normalized rolled
  - capital letter **L** for the qualities with specified impact properties at – 50°C
  - capital letter **H** to indicate hollow sections

EXAMPLE Structural steel (S) with a specified minimum yield strength for a thickness not greater than 16 mm of 355 MPa, normalized condition (N), with a minimum impact energy value of 27 J at -50 °C (L), hollow section (H): EN 10210-S355NLH

From the two available hot finished hollow section the author chose fine grain steel sections which are produced by "Tata steel" and their detailed dimensions and sectional properties found in their website [5] manufactured according to EN10210-2 [4].

1.2 Scope of the Study

The scope of the study has been limited to evaluating hot finished hollow section columns for the Steel grade of S235NH, S275NH, S275NLH, S355NH and S355NLH. All cross sections investigated are at least class 3 to avoid local buckling. Hollow sections response for axial compression was investigated. Torsion, moment and shear and second order effects are not parts of the study. Circular hollow sections are not the part of the study because they have same stiffness on both directions. Cold formed sections are also not the part of the study because there is no recommended residual stress on ECCS[6] as that of the hot finished one but the author use cold formed sections for validation works of Finite Element simulation and their residual stress is properly measured and stated on key and Hancock[7]. Most modern structural analysis programs now have the ability to perform

second order elastic analysis. Due to computational time the Finite element models are limited in number.

1.3 Objectives of the Thesis

The prime aim of this thesis has been to study buckling load and flexural buckling curves for hot-rolled hollow sections.

The main goals can be subdivided into further sub-sections consisting in:

- To discuss the theoretical background of flexural buckling curve formulae given in EN 1993-1-1 [8].
- To validate the FEM analysis with experimental result and to select mesh size and geometric imperfection for FEA and also the effect of residual stress on buckling load of columns.
- To examine and select suitable material behavior recommended in EN 1993-1-5 [9] for FEA.
- To assess the effect of varying the ratio of height to width (H/B) when performing flexural buckling curves in both major and minor axis for rectangular hot rolled hollow sections.

CHAPTER 2 LITERATURE REVIEW

2.1 Structural Stability

The buckling resistance theory of compressed elements in steel structures has a varied history. Despite the many investigations in recent decades, research still seeks to define the actual behavior of the columns by experimental and numerical analyses.

2.1.1 Structural stability and equilibrium

The structural design must consider not only safety and strength criteria but also stability, especially for slender members. Considering a structure under an external loading that presents a specific equilibrium configuration, the stability of this configuration is evaluated through the structural behavior after a small perturbation caused by an external force. Figure 2-1 illustrates the three equilibrium states: (a) stable, if the structure returns to its initial position, (b) unstable, if it does not and (c) neutral, if it remains indifferent.

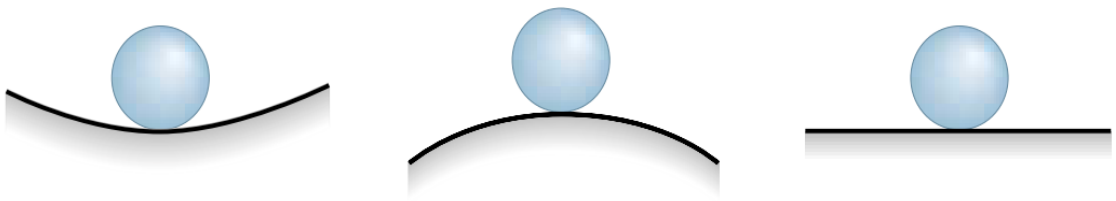

Figure 2-1: The three equilibrium states: (a) stable; (b) unstable; (c) neutral

The instability of a structure progresses along an equilibrium path and passes through a transition from a stable to an unstable equilibrium configuration. This instability phenomenon associated with an equilibrium bifurcation is called bifurcation instability.

2.1.2 Elastic buckling

The column buckling theory has begun in 1774 with the publication of the first work of L. Euler. In this work, it has been determined the useful elastic limit for a perfect column due to large displacements under the critical load $N_{cr}=\pi^2.B/L^2$ where the term B initially was defined as the absolute elasticity and, after 1775, as the stiffness. Only in his third work, in 1778, Euler finally introduced the classic formula and defined the term B as the

flexural rigidity (EI), where E is the modulus of elasticity or Young modulus and I is the moment of inertia of the cross-section.

$$P_{cr} = \frac{n^2 \pi^2 EI}{L^2} \tag{2.1}$$

As we see from Eq. (2.1) the buckling load depends on flexural stiffness (EI), for steel section modulus of elasticity (E) is constant and stiffness varied from sections to sections by Second moment of inertia (I). The critical buckling depends on the second moment of inertia (I), we get different buckling load for every variation of moment of Inertia (I). Even in one section we can get a different moment of Inertia (I) for the strong and weak axis. Based on this assumption EN 1993-1-1 [8] provide flexural buckling Curves for the section with both minor and major axis.

2.1.3 Ultimate strength

The real behavior of steel columns is rather different from that described in the previous section and columns generally fail by inelastic buckling before reaching the Euler buckling load. The difference in real and theoretical behavior is due to various imperfections in the "real" element: initial out-of-straightness, residual stresses, eccentricity of axial applied loads and strain-hardening. All imperfections affect buckling and will, therefore, influence the ultimate strength of the column. Experimental studies of real columns give results as shown in Figure 2-2 represented by “x” symbols. Compared to the theoretical curves, the real behavior shows greater differences in the range of medium slenderness than in the range of large slenderness. The lower bound curve is obtained from a statistical analysis and represents the safe limit for loading [10].

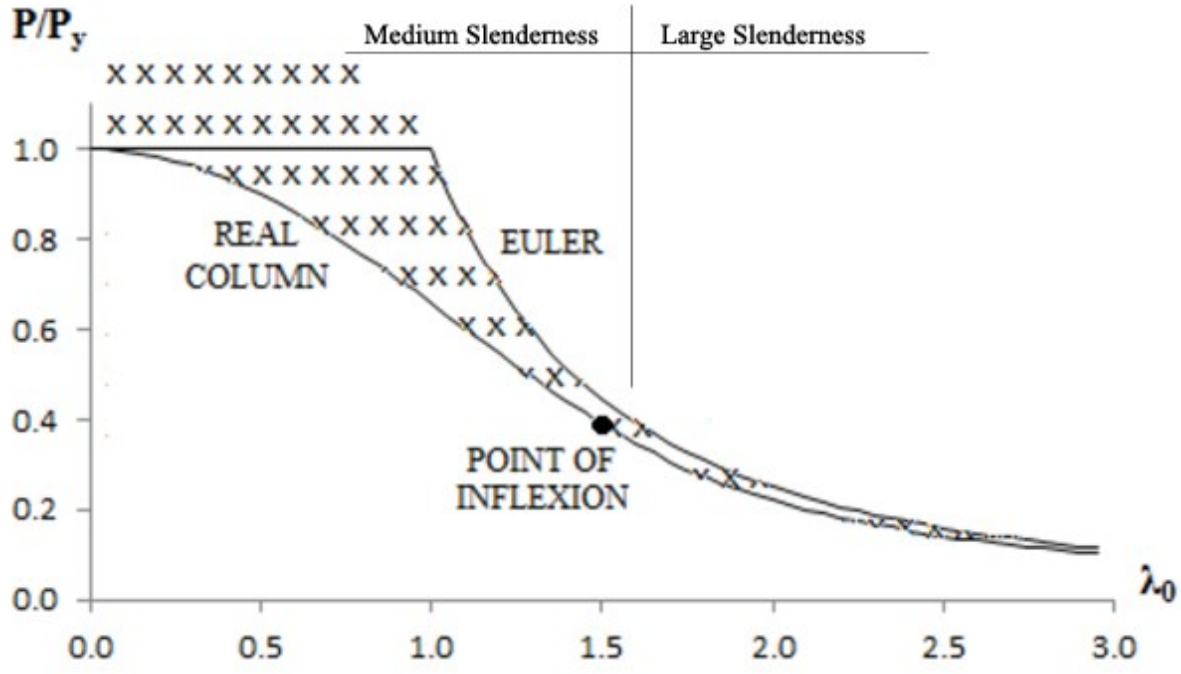

Figure 2-2: Real column and Euler curves

2.1.4 Reduction factor

The derivation of the reduction factor, χ, for a simple case can be made from second-order analysis done above. Consider the illustration as shown in Figure 2-3 of a simply supported member under pure axial compression with an initial transverse deflection [11].

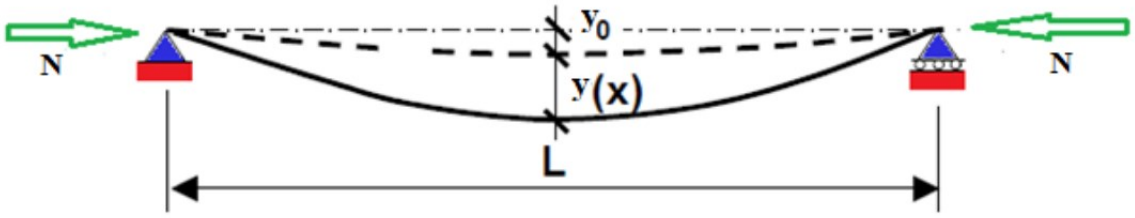

Figure 2-3: Column buckling in pure axial compression.

Assuming a sinusoidal deflection, the initial geometrical imperfection can be expressed as:

$$y_0(x) = e_0 \sin\left(\frac{\pi . x}{L}\right) \tag{2.2}$$

When an axial force N is applied to the column, the additional deflection associated to instability can be expressed as:

$$y(\mathrm{x}) = A\sin(\frac{\pi.\mathrm{x}}{L}) \tag{2.3}$$

The classical buckling equilibrium Eq. for this case then is:

$$y'' + \frac{N}{EI}(y_0(x)) + y(x) = 0 \tag{2.4}$$

Inserting Eqs. (2.2) and (2.3) into Eq. (2.4) and evaluating:

$$A = \frac{N}{N_{cr} - N} e_0 \tag{2.5}$$

where: N_{cr} is the elastic buckling load i.e. the Euler load.

Thus, Eq. (2.3) is re-written as:

$$y(\mathrm{x}) = \frac{N}{N_{cr} - N} \mathrm{e}_0 \sin(\frac{\pi\,\mathrm{x}}{L}) \tag{2.6}$$

At mid span, the total deflection is expressed as:

$$y_{\max} = \frac{N}{N_{cr} - N} e_0 \tag{2.7}$$

The member cross-section's resistance criterion at mid-span including second order effects is then expressed as:

$$\frac{N}{Af_y} + \frac{1}{1 - \frac{N}{N_{cr}}} . \frac{N.e_0}{M_{ed}} \le 1 \tag{2.8}$$

where: M_e is the bending moment.

Let,

$$Af_y = N_{Rd} \tag{2.9}$$

where: N_{Rd} is the design values of resistance to normal forces.

The buckling resistance, N_{Rd}, is expressed as:

$$N_{b.Rd} = \chi N_{Rd} \tag{2.10}$$

where: χ is called the reduction factor.

$N_{b,Rd}$ is the design buckling resistance.

Non-dimensional slenderness is expressed as:

$$\bar{\lambda}^2 = \frac{Af_y}{N_{cr}} = \frac{N_{Rd}}{N_{cr}} \tag{2.11}$$

The bending moment is the product of the yield force and elastic modulus, W_{el}, and is expressed as:

$$M_{ed} = W_{el} f_y \tag{2.12}$$

where: M_{ed} is called the design bending moment.

At buckling, the maximum applied axial force reaches the actual buckling resistance, thus:

$$N = N_{b.Rd} = \chi N_{Rd} \tag{2.13}$$

Inserting Eqs. (2.9), (2.10), (2.11), (2.12) and (2.13) into Eq. (2.8), then:

$$\frac{\chi N_{Rd}}{N_{Rd}} + \frac{1}{1-\chi\frac{N_{Rd}}{N_{cr}}} \cdot \frac{\chi N_{Rd}.e_0}{W_{el} f_y} \le 1 \tag{2.14}$$

$$\chi + \frac{1}{1-\chi.\bar{\lambda}^2} \cdot \frac{\chi A f_y.e_0}{W_{el} f_y} \le 1$$

$$\chi + \frac{1}{1-\chi.\bar{\lambda}^2} \cdot \frac{\chi A.e_0}{W_{el}} \le 1$$

Solving for χ in Eq. (2.14)

Let,

$$\frac{A.e_0}{W_{el}} = \eta \tag{2.15}$$

Thus, $\chi + \frac{1}{1-\chi.\bar{\lambda}^2}.\eta\chi = 1$

After rearrangement, a second order of polynomial is obtained as:

$$\chi^2\bar{\lambda}^2 - (1+\eta+\bar{\lambda}^2)\chi + 1 = 0 \tag{2.16}$$

Solving the quadratic Eq. (2.16) will give out two solutions. The lower value is taken to be the reduction factor, therefore:

$$\chi = \frac{(1+\eta+\bar{\lambda}^2) - \sqrt{(1+\eta+\bar{\lambda}^2)^2 - 4\bar{\lambda}^2}}{2\bar{\lambda}^2} \tag{2.17}$$

Let, $0.5(1+\eta+\bar{\lambda}^2) = \Phi$

Therefore:

$$\chi = \frac{\Phi - \sqrt{\Phi^2 - \bar{\lambda}^2}}{\bar{\lambda}^2} \tag{2.18}$$

Multiplying Eq. (2.18) with $\Phi + \sqrt{\Phi^2 - \bar{\lambda}^2}$, thus:

$$\chi = \frac{1}{(\Phi + \sqrt{\Phi^2 - \bar{\lambda}^2})} \tag{2.19}$$

Eq. (2.19) is the reduction factor which is identical to Eq. (2.20) given in EN 1993-1-1.

2.2 Strength Curves

Numerous research works on compressive strength of columns conducted in North America and Europe since 1970 have resulted in the concept of multiple buckling curves to cover the full range of sections, steel grades and manufacturing processes used in construction industry. The European column buckling curves are based on extensive experimental research programs as well as theoretical, numerical and probabilistic investigations performed around the 1960s and early 1970s. Standardized buckling tests were performed at different laboratories and the gathered parametric information and results were analyzed using both probabilistic and deterministic methods.

In 1975 Dwight [12] reports on the work towards incorporating the "Ayrton-Perry" approach including equivalent imperfections and a plateau corresponding to relative slenderness values lower than λ_0=0.2. In the 1984 report on Eurocode 3 by Dowling et al. [13] the "Ayrton-Perry" approach was included for simple member verification as well as the possibility of numerical verification using 1/1000 of the buckling length L, as initial bow imperfection with simplified linear residual stress distributions. Furthermore, an equivalent geometric imperfection dependent on the buckling curve of the cross-section could be used. The simplified residual stress distributions including tubes were also given in the ECCS report on sway frames [6]. In the 1992 draft for development of Eurocode 3 [8] the Ayrton-Perry approach was included with a somewhat cumbersome awkward mix of definitions of the equivalent imperfections dependent on safety factors and on whether strong or weak axis was being analyzed. In the case of strong axis buckling the equivalent imperfection was more or less extracted directly from the "Ayrton-Perry" based buckling curve. In case of weak axis buckling an equivalent imperfection was given as a fraction of the buckling length, but including a correction factor removing the (correct) influence of the yield stress. In this preliminary Eurocode 3 the previous proposal of allowing the use of assessment with residual stress and related bow imperfection was not included.

From 1992 until 2005 when the EN 1993-1-1 [8] finally became a harmonized European standard the buckling curve formulation remained nearly unchanged. The European EN 1993-1-1 [8] adopts the concept of multiple strength curves. They are five: a_0, a, b, c and d, for different cross-sections. The curves are expressed by:

$$\chi = \frac{1}{\Phi + \sqrt{\Phi^2 - \bar{\lambda}^2}} \leq 1.0 \tag{2.20}$$

where

$$\Phi = 0.5 \cdot [1 + \alpha(\bar{\lambda} - 0.2) + \bar{\lambda}^2] \tag{2.21}$$

Table 2-1: Imperfection factors for buckling curves [8]

Buckling curve	a_0	a	b	c	d
Imperfection factor α	0,13	0,21	0,34	0,49	0,76

Table 2-2: Buckling curve selection [8]

Cross section		Limits	Buckling about axis	Buckling curve	
				S 235 S 275 S 355 S 420	S 460
Hollow sections		hot finished	any	a	a_0
		cold formed	any	c	c

As we seen in Table 2-2 buckling curves for square and rectangular sections is the same but the rectangular sections have different stiffness in the strong and minor axis.

2.3 Finite Element Model

2.3.1 General remarks

There are many parameters that control the choice of finite element type and mesh such as the geometry, cross section classification, loading, and boundary conditions of the structural member. Accurate finite element modeling depends on the efficiency in simulating the nonlinear material behavior of metal structural members. Most of metal structures have initial local and overall geometric imperfections as well as residual stresses as a result of the manufacturing process. Ignoring the simulation of these initial imperfections and residual stresses would result in poor finite element models that are unable to describe the performance of the metal structure [14]. In addition, there are

different loads and boundary conditions applied to metal columns. Improper simulation of applied loads and boundary conditions on a structural member would not provide an accurate finite element model. Therefore, correct simulation of different loads and boundary conditions that are commonly associated with metal structural members is highlighted.

2.3.2 Choice of element type for metal structures

Finite element models are normally developed to perform different analyses and parametric studies on different cross sections; hence, it is recommended to choose 3D *elements* in modeling the rectangular and square hollow section columns.

The 3D *elements, brick, or solid elements* are often used to model metal structures that are loaded by forces in 3D named three-dimensional stress analysis.

The naming conventions for solid elements depend on the element dimensionality, number of nodes in the element, and integration type. For example, C3D8R elements are continuum elements (C), 3D elements having eight nodes with reduced integration (R). Solid elements provide accurate results if not distorted, particularly for quadrilaterals and hexahedra [14]. Solid element library includes first-order (linear) interpolation elements and second-order (quadratic) interpolation elements commonly in three dimensions. Tetrahedral, triangular prisms, and hexahedra (bricks) are very common 3D elements.

2.3.3 Choice of finite element mesh for metal structures

After choosing the best finite element type to model a metal structural member, we need to look into the geometry of the metal structural member to decide the best finite element mesh. Normally, most cold formed and hot-rolled metal structural members have flat and curved regions. Therefore, the finite element mesh has to cover both flat and curved regions. Also, most metal structural members have short dimensions, which are commonly the lateral dimensions of the cross section, and long dimensions, which are the longitudinal axial dimension of the structural member that defines the structural member length. Therefore, the finite element mesh has to cover both lateral and longitudinal regions of the structural member. To mesh the column correctly, we have to start with a short dimension for the chosen shell element and decide the best aspect ratio.

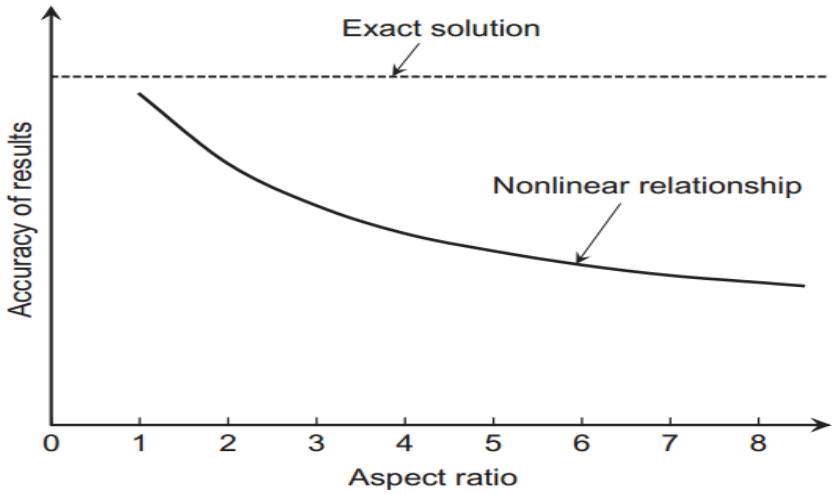

Figure 2-4: Effect of aspect ratio of finite elements on the accuracy of results.

The aspect ratio is defined as the ratio of the longest dimension to the shortest dimension of a quadrilateral finite element. As the aspect ratio is increased, the accuracy of the results is decreased. The aspect ratio should be kept approximately constant for all finite element analyses performed on the column. Therefore, most general-purpose finite element software specify a maximum value for the aspect ratio that should not be exceeded; otherwise, the results will be inaccurate. Figure 2-4 presents a schematic diagram showing the effect of aspect ratio on the accuracy of results. The best aspect ratio is 1, and the maximum value, as an example the value recommended by ABAQUS [15], is 5.

2.4 Residual Stress

Residual stress refers to a stress distribution, which is present in a structure, component, plate or sheet, while there is no external load applied. In view of the absence of an external load, the residual stresses are sometimes labeled as internal stresses. The background of the terminology “residual stress” is that residual stress distribution in a material is often left as a residue of inhomogeneous plastic deformation. Residual tensile stress and residual compressive stress always occur together [16].

Key and Hancock [7] studied the influence of residual stresses components on the axial compression behavior of thick carbon steel hollow sections. Their measurements were able to show the complex through-thickness residual stress distribution. The measured residual

stresses components in both the longitudinal and transverse directions were included progressively in the finite strip analysis of stub column behavior. Key and Hancock [7] proposed models for the through-thickness variation as shown in Figure 2-5.

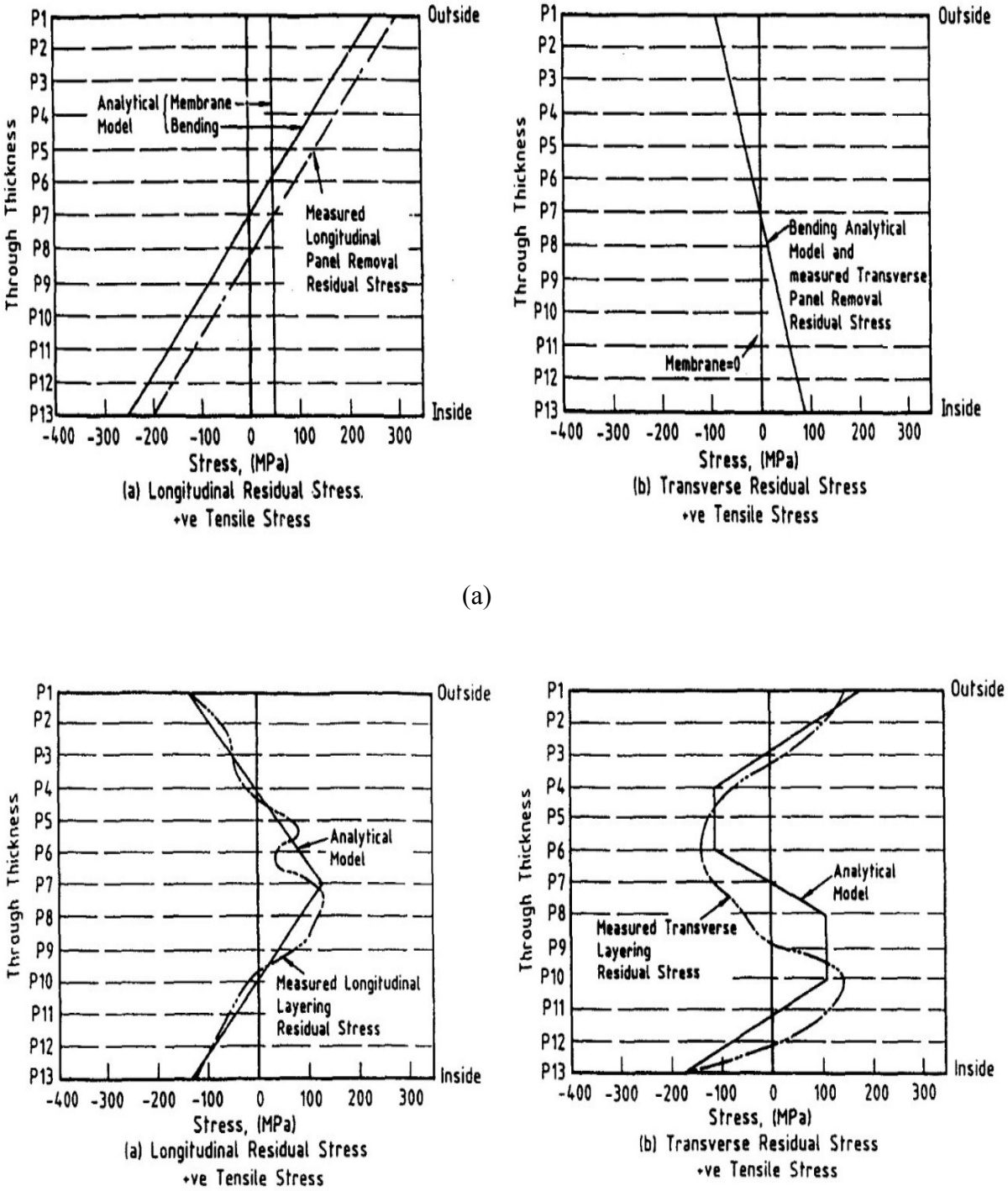

Figure 2-5: Analytical models for through-thickness residual stresses; (a) analytical model for panel removal residual stress, (b) analytical model for layering residual stresses. [7]

Key and Hancock [7] concluded that the longitudinal membrane residual stresses component had a negligible influence on the section behavior, whereas flexural residual stresses which varied linearly through the plate thickness affected the results and the ultimate load as well as the axial stiffness. The addition of the layering residual stresses induced a small influence on the ultimate load, but the axial stiffness was reduced at an early stage.

Cruise and Gardner [17] reported that for the press braked sections, the membrane and bending residual stresses in the unformed flat regions were generally low, typically below 10% of the material 0.2% proof strength. In the corner regions, however, where large plastic deformation occurs, higher bending residual stresses were observed. The corner bending residual stresses typically reached about 30% of the corner material 0.2% proof strength, which itself has been enhanced beyond the strength of the flat material due to cold work during production. For the cold rolled sections, the results reveal slightly higher membrane residual stresses than those observed in the hot rolled and press braked sections, and considerably higher bending residual stresses. The bending residual stresses that were measured typically ranged between about 30% and 70% of the material 0.2% proof stress.

Gardner and Saari [18] reported that the mean value of the normalized bending residual stresses for the flat faces of the cold-formed box sections was found to be slightly higher than that of the corner regions. Similar patterns were observed for cold-formed stainless steel box sections [17].

Tong [19] examined experiment and his results indicate that the longitudinal residual stresses are in tension at outer surface and in compression at inner surface, and present nonlinear distributions along the section thickness. Longitudinal residual stresses are small at the middle-surface along the thickness of the section. It is also shown that the magnitudes of the longitudinal residual stresses at the corner parts are larger than those at flat parts.

Zhang [20] reported that for residual stresses in the transverse direction, the cold-formed SHS clearly contains the highest level, especially at the corner and welding areas. The transverse residual stresses in the corner of the cold-formed SHS is compressive stresses while those in the flat and welding area are tensile stresses. The “highest” stress in the

corner is −20.1% of actual yield strength while the highest tensile stresses in the flat and welding area are 32.2% and 31.3%, respectively.

Somodi and Kövesdi [21] developed their residual stress model and reported that the residual stress developed in corner is 55% of the flat one but residual stress model is only applicable for specimens produced by the "continuous forming" manufacturing method,- the model can be applied for HSS square hollow sections using steel grades of S500–S960 (for normal steel grades it can give significant overestimation of the residual stresses).

The commonly used residual model in hot-rolled sections based on ECCS [6] recommendations were adopted and also introduced in the numerical model of this investigation due to its simplicity and commonly used.

CHAPTER 3 MATERIALS, METHODS AND PROCEDURES

3.1 Elements

The geometrical and material non-linear analyses on the columns containing imperfections (GMNIA) were performed in the ABAQUS v.6.14. The columns were modeled with brick elements. The 8-node linear brick, reduced integration (C3D8R) recommended in ABAQUS manual and was selected for the analyses as it can describe plasticity, large deformations and large strains.

ABAQUS has no built-in system of units. Therefore, it is important to define all the input data in consistent units. The SI system of units is used throughout this project as shown in the following table.

Table 3-1: SI Units.

Quantity	**SI units**
Length	M
Force	N
Mass	Kg
Time	S
Stress	Pa (N/m^2)
Energy	J
Density	kg/m^3

3.2 Material Modeling

In accordance with the classification system in EN 10020 [22], steel grades S275NH, S275NLH, S355NH and S355NLH are non-alloy quality steels and steel grades. EN 10210-1 [3] gives nominal values of yield strength fy for hot finished hollow section.

Table 3-2: Mechanical properties of fine grain structural steel hollow sections. [3]

Steel grade		Minimum yield strength R_{eH} MPa			Tensile strength R_m MPa
Steel name	Steel number	Specified thickness mm			at specified thickness ≤ 65 mm
		≤ 16	> 16 ≤ 40	> 40 ≤ 65	
S275NH	1.0493	275	265	255	370–510
S275NLH	1.0497				
S355NH	1.0539	355	345	335	470–630
S355NLH	1.0549				
S420NH	1.8750	420	400	390	520-680
S420NLH	1.8751				
S460NH	1.8953	460	440	430	540–720
S460NLH	1.8956				

The elastic modulus, E, (i.e. the inclination of the stress-strain curve), is also an important parameter, which corresponds to a mean value that in EN 1993-1-1 [8] is always set to be 210 GPa. Annex C of EN 1993-1-5 [9] recommends the use of one of the following three material behavior models when performing plated finite element analysis:

a) elastic–plastic without strain hardening

b) elastic–plastic with a nominal plateau slope of 1 MPa

c) elastic–plastic with a strain hardening slope of E/100

Figure 3-1 shows the nominal stress-strain curves, for an elastic material and for the elastic plastic material, which were utilized to calculate the values of the true stresses and true strains.

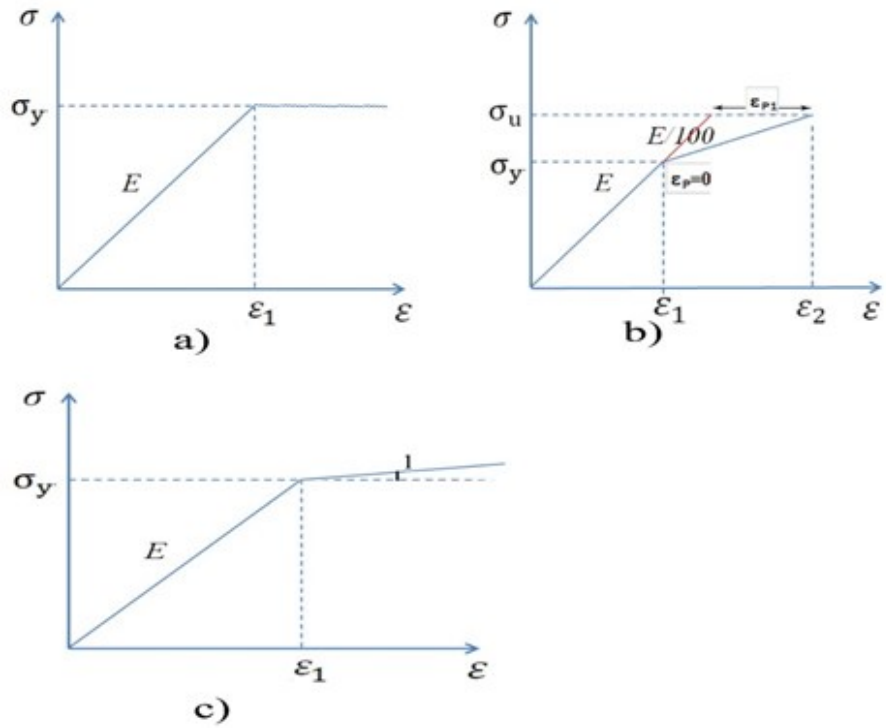

Figure 3-1: Nominal stress-strain curves, where a) is for purely elastic material and b) is for elastic plastic material with a strain hardening slope of E/100 c) is for elastic plastic material with a nominal plateau slope of 1 MPa.

Elastic-plastic with a strain hardening slope of E/100

The true strain or the logarithmic strain is a mathematical model which describes the plastic behavior of the metals which accounts for differences in the compression and tensile behavior independent of the structure's geometry or nature of the load applied. In ABAQUS, when plasticity of the material data is defined, true stress and true strain should be used. These are the values that ABAQUS need to correctly interpret the data. The nominal stress and strain values are often supplied by the material test data. However, the material plasticity data must be converted from the nominal stress and nominal strain values to the true stress and true strain values respectively.

The plastic properties are computed using the following relationships

$$\sigma_{true} = \sigma(1+\varepsilon) \tag{3.1}$$

$$\varepsilon_{true} = \ln(1+\varepsilon) \tag{3.2}$$

where ε is nominal strain

σ is nominal stress

σ_{true} is the true stress

ε_{true} is the true strain

To calculate the strain the values of the yield strength and ultimate strength Table 3-1 are used, thus:

From Figure 3-1a, since the slope is, for the elastic region, thus,

$$(355x10^6 - 0) = \mathrm{E}(\varepsilon_1 - 0)$$

Therefore: $\varepsilon_1 = \dfrac{355x10^6}{210x10^9} = 0.0016$

For the plastic region, the slope is *E/100*. see Figure 3-1b. Thus,

$$(470x10^6 - 355x10^6) = \left[E/100\right](\varepsilon_2 - \varepsilon_1)$$

Therefore: $\varepsilon_2 = \dfrac{100x115x10^6}{210x10^9} + 0.0016 = 0.0565$

Utilizing Eq. (3.1) and (3.2), the true yield strength is:

$$\sigma_{ytrue} = \sigma_y(1+\varepsilon_1)$$

$$\sigma_{ytrue} = 355x10^6(1+0.0016) = 355.6001MPa$$

and the true ultimate strength is:

$$\sigma_{utrue} = \sigma_u(1+\varepsilon_2)$$

$$\sigma_{utrue} = 470x10^6(1+0.0565) = 496.5644\,\mathrm{MPa}$$

Table 3-3: Stress and Strain values for S355.

	Nominal Strain	Engineering Stress (Mpa)	True Strain	True Stress (Mpa)	Strain for nonlinear analysis
1	0.0016	355.000	0.0016	355.6001	0.0000
2	0.0564	470.000	0.0549	496.5326	0.0525

The above calculation is for a steel grade S355, for the rest of steel grades are summarized in Table 3-4.

Table 3-4: Stress and Strain values with a strain hardening slope of E/100 and Elastic-plastic with a nominal plateau slope of 1 MPa for S275, S355, S420 and S460.

	Elastic-plastic with a strain hardening slope of E/100		Elastic-plastic with a nominal plateau slope of 1 Mpa	
Steel Grade	True Stress (Mpa)	True Strain	True Stress (Mpa)	True Strain
S275	275.3601	0.0000	275.0000	0.0000
	387.2226	0.0437	286.1739	0.2487
S355	355.6001	0.0000	355.0000	0.0000
	496.5326	0.0527	366.1739	0.2483
S420	420.8400	0.0000	420.0000	0.0000
	545.8019	0.0460	431.1739	0.2480
S460	461.0076	0.0000	460.0000	0.0000
	561.7543	0.0369	471.1739	0.2478

The values in Table 3-4 was used for the non-linear analysis and Compare with Elastic-plastic without strain hardening.

3.3 Initial Imperfections

Most hot-rolled metal structural members have initial geometric imperfections as a result of the manufacturing, transporting, and handling processes. Initial geometric imperfections can be classified into two main categories, which are local and overall (bow, global, or out-of-straightness) imperfections. Initial local geometric imperfections can be found in any region of the outer or inner surfaces of metal structural members and are in

the perpendicular directions to the structural member surfaces. On the other hand, initial overall geometric imperfections are global profiles for the whole structural member along the member length in any direction. Initial local and overall geometric imperfections can be predicted from finite element models by conducting eigenvalue buckling analysis to obtain the worst cases of local and overall buckling modes.

Accurate finite element models must incorporate initial local and overall geometric imperfections in the analysis, otherwise, the results will not be accurate. Even in most axially loaded metal long column tests, the columns tend to buckle in the direction of the maximum initial overall geometric imperfection. In addition, in most eccentrically loaded metal long column tests, the initial overall geometric imperfection must be added to the eccentricity to obtain the moment resistance of the column.

The shape of the geometric imperfection will be based on the buckling mode belonging to the lowest eigenvalue from a linear buckling analysis. This resulted in a sinusoidal bow imperfection. The amplitude defining the maximum deviation from the ideal geometry will L/1000, where L is the height of the column. This approach is generally accepted for the determination of buckling curves. The value L/1000 for the imperfection amplitude is recommended in [6]. The value L/1000 is a design imperfection amplitude for use in numerical analyses and adopted in this work.

3.4 Residual Stresses

Residual stresses have been introduced in the models. Residual stresses based on ECCS [6] recommendations were adopted and also introduced in the numerical model of this investigation. A typical approximation of residual stress patterns frequently used in advanced structural analysis consists in the trapezoidal shape shown in Figure 3-2. Based on these recommendations, a proposal with $0.5f_y$[1] at the corners was assumed and the corresponding values needed to reach equilibrium in flanges and webs were calculated by means of usual structural mechanics equations.

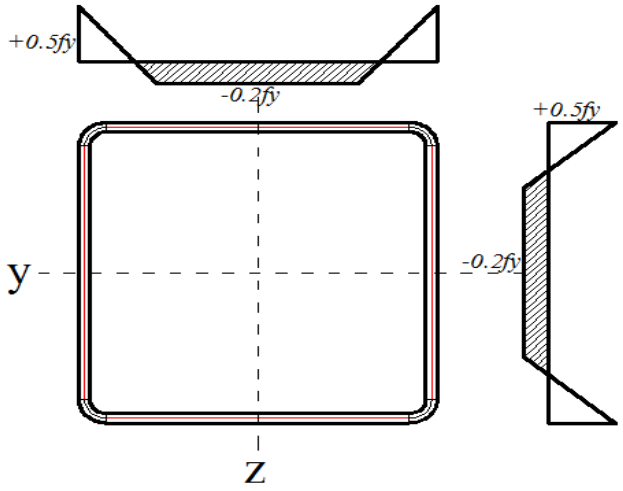

Figure 3-2: ECCS recommendations for residual stresses.[6]

3.5 Boundary Conditions

Following the load application on the finite element model, we can now apply the boundary conditions on the finite element model. Boundary conditions are used in finite element models to specify the values of all basic solution variables such as displacements and rotations at nodes. Boundary conditions can be given as model input data to define zero-valued boundary conditions and can be given as history input data to add, modify, or

[1] f_y refers to a conventional yield stress of 235 N/mm^2.

.

remove zero-valued or nonzero boundary conditions. Boundary conditions can be specified using either *direct format* or *type format*. The type format is a way of conveniently specifying common types of boundary conditions in stress-displacement analyses. Direct format must be used in all other analysis types. For both direct and type format, the region of the model to which the boundary conditions apply and the degrees of freedom to be restrained must be specified.

Boundary conditions prescribed as model data can be modified or removed during analysis steps. In the direct format, the degrees of freedom can be constrained directly in the finite element model by specifying the node number or node set and the degree of freedom to be constrained. As an example in ABAQUS, when you specify that "PINNED" means pin-ended case, which implies that the degrees of freedom 1, 2, and 3 equal to 0.

The application of boundary conditions is very important in finite element modeling. The application must be identical to the actual situation in the metal structural member test or construction. Otherwise, the finite element model will never produce accurate results.

All selected column configurations for the present investigations were simply supported. The column was pin-supported and torsionally restrained at the bottom. The same boundary condition was applied at the top with the exception that vertical translation was permitted. For the evaluation of strong-axis buckling, the column was restrained against weak-axis deflections by translational supports along the length to prevent from failing in weak-axis (Figure 3-3).

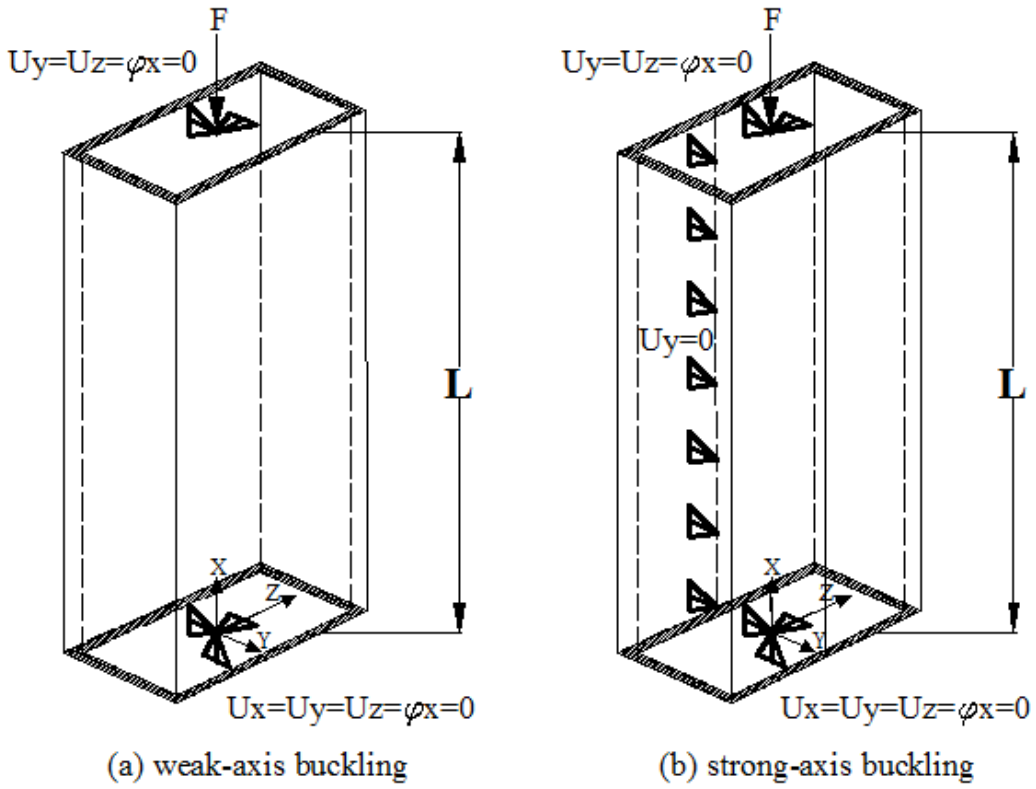

Figure 3-3: Boundary conditions.

3.6 Analysis Procedures

Most available general-purpose finite element software divides the problem history (overall finite element analysis) into different steps as shown in Figure 3-4.An analysis procedure can be specified for each step, with prescribing loads, boundary conditions, and output requests specified for each step. A step is a phase of the problem history, and in its simplest form, a step can be just a static analysis of a load changing from one magnitude to another, as shown in Figure 3-4. For each step, one can choose an analysis procedure. This choice defines the type of analysis to be performed during the step such as static stress analysis, eigenvalue buckling analysis, or any other types of analyses.

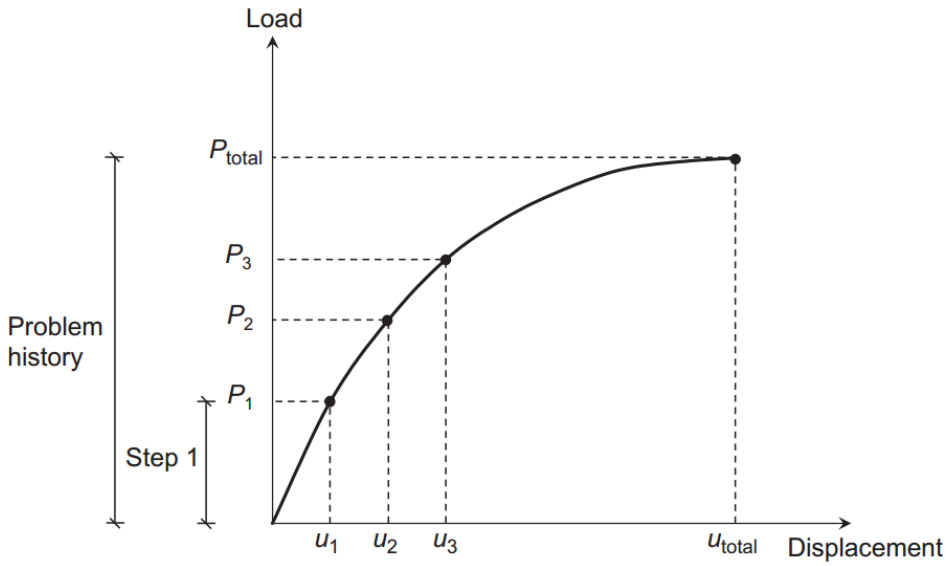

Figure 3-4: Load-displacement history in a nonlinear analysis.

They also classify the steps into two main kinds of steps: general analysis steps and linear perturbation steps. General analysis steps can be used to analyze linear or nonlinear response. On the other hand, linear perturbation steps can be used only to analyze linear problems. Linear analysis is always considered to be linear perturbation analysis about the state at the time when the linear analysis procedure is introduced.

It should be noted that linear perturbation steps have no effect on subsequent general analysis steps and can be conducted separately as a whole (overall) analysis procedure. In this case, the data obtained from the linear perturbation steps can be saved in files that can be called into the subsequent general analysis steps. For example, linear eigenvalue buckling analyses, needed for modeling of initial overall and local geometric imperfections, can be conducted initially as a separate overall analysis procedure, and buckling modes can be extracted from the analyses and saved in files. The saved files can be called into subsequent static general analyses and factored to model initial geometric imperfections.

They software divides each step of analysis into multiple increments. In most cases, one can choose either automatic (direct) time incrementation or user-specified fixed time incrementation to control the solution. Automatic time incrementation is a built-in incrementation scheme that allows the software to judge the increment needed based on equilibrium requirements. On the other hand, user-specified fixed time incrementation

forces the software to use a specified fixed increment, which in many cases may be large, small, or need updating during the step. This results in the analysis to be stopped and readjusted. Therefore, automatic incrementation is recommended for most cases.

3.6.1 Linear eigenvalue buckling analysis

Eigenvalue buckling analysis is generally used to estimate the critical buckling (bifurcation) load of structures. The analysis is a linear perturbation procedure. The analysis can be the first step in a global analysis of an unloaded structure or it can be performed after the structure has been preloaded. It can be used to model measured initial overall and local geometric imperfections or in the investigation of the imperfection sensitivity of a structure in case of lack of measurements. Eigenvalue buckling is generally used to estimate the critical buckling loads of stiff structures (classical eigenvalue buckling). Stiff structures carry their design loads primarily by axial or membrane action, rather than by bending action. Their response usually involves very little deformation prior to buckling.

The buckling loads are calculated relative to the original state of the structure. If the eigenvalue buckling procedure is the first step in an analysis, the buckled (deformed) state of the model at the end of the eigenvalue buckling analysis step will be the updated original state of the structure. The eigenvalue buckling can include preloads such as dead load and other loads. The preloads are often zero in classical eigenvalue buckling analyses. An incremental loading pattern is defined in the eigenvalue buckling prediction step. The magnitude of this loading is not important; it will be scaled by the load multipliers that are predicted by the eigenvalue buckling analysis. The buckling mode shapes (eigenvectors) are also predicted by the eigenvalue buckling analysis. The critical buckling loads are then equal to the preloads plus the scaled incremental load. Normally, the lowest load multiplier and buckling mode are of interest. The buckling mode shapes are normalized vectors and do not represent actual magnitudes of deformation at critical load. They are normalized so that the maximum displacement component has a magnitude of 1.0. If all displacement components are zero, the maximum rotation component is normalized to 1.0. These buckling mode shapes are often the most useful outcome of the eigenvalue buckling analysis, since they predict the likely failure modes of the structure.

Boundary conditions can be applied to any of the displacement or rotation degrees of freedom (six degrees of freedom). Boundary conditions are treated as constraints during the eigenvalue buckling analysis. Therefore, the buckling mode shapes are affected by these boundary conditions. The buckling mode shapes of symmetric structures subjected to symmetric loadings are either symmetric or antisymmetric. In such cases, it is more efficient to use symmetry to reduce the finite element mesh of the model.

All nonlinear or inelastic material properties are ignored during an eigenvalue buckling analysis. Any structural finite elements can be used in an eigenvalue buckling analysis. The values of the eigenvalue load multiplier (buckling loads) will be printed in the data files after the eigenvalue buckling analysis. The buckling mode shapes can be visualized using the software. Any other information such as values of stresses, strains, or displacements can be saved in files at the end of the analysis.

3.6.2 Materially nonlinear analysis

Materially nonlinear analysis of metal structures is a general nonlinear analysis step. The analysis can be also called load-displacement nonlinear material analysis and normally follows the linear eigenvalue buckling analysis step or initial condition stress analysis. All required information regarding the behavior of metal structures are predicted from the materially nonlinear analysis. The information comprised the ultimate loads, failure modes, and load-displacement relationships, as well as any other required data, can be obtained from materially nonlinear analysis. The initial overall and local geometric imperfections, residual stresses, and nonlinear stress-strain curves of the construction material are included in the load-displacement nonlinear material analysis.

Materially nonlinear analysis (with or without consideration of geometric nonlinearity) of metal structures is done to determine the overall response of the structures. From a numerical viewpoint, the implementation of a nonlinear stress-strain curve of a construction metal material involves the integration of the state of the material at an integration point over a time increment during a materially nonlinear analysis. The implementation of a nonlinear stress-strain curve must provide an accurate material stiffness matrix for use in forming the nonlinear equilibrium equations of the finite element formulation.

The mechanical constitutive models associated with metal structures in ABAQUS consider elastic and inelastic response of the material. The inelastic response is commonly modeled with plasticity models as mentioned previously. In the inelastic response models that are provided in ABAQUS, the elastic and inelastic responses are distinguished by separating the deformation into *recoverable* (elastic) and *nonrecoverable* (inelastic) parts. This separation is based on the assumption that there is an additive relationship between strain rates of the elastic and inelastic parts.

The constitutive models obtain the state at the point under consideration at the start of the increment from the material database specified in the step. The state variables include the stresses and strains used in the constitutive models. The constitutive models update the state of the material response to the end of the increment.

3.6.3 Geometrically nonlinear analysis

Geometrically nonlinear analysis of metal structures is a general nonlinear analysis step. The analysis can be also called load-displacement nonlinear geometry analysis and normally follows the linear eigenvalue buckling analysis step or initial condition stress analysis. The initial overall and local geometric imperfections and residual stresses are included in the load-displacement nonlinear geometry analysis. If the stress-strain curve of the construction metal material is nonlinear, the analysis will be called combined materially and geometrically nonlinear analysis or load-displacement nonlinear material and geometry analysis.

All required information regarding the behavior of metal structures are predicted from the combined materially and geometrically nonlinear analysis. The information comprised the ultimate loads, failure modes, and load-displacement relationships, as well as any other required data, can be obtained from the combined materially and geometrically nonlinear analysis.

3.6.4 Riks method

The Riks method provided by ABAQUS is an efficient method that is generally used to predict unstable, geometrically nonlinear collapse of a structure. The method can include nonlinear materials and boundary conditions. The method commonly follows an eigenvalue buckling analysis to provide complete information about a structure's collapse.

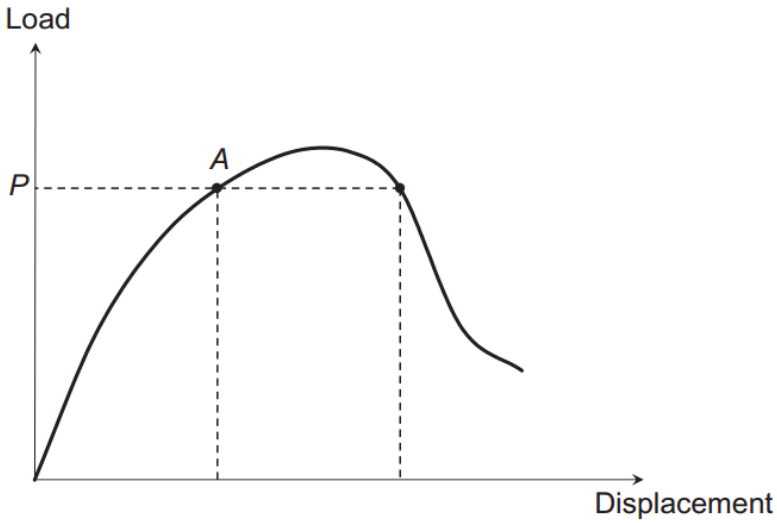

Figure 3-5: Load-displacement behavior that could be predicted by the Riks method

The Riks method treats the load magnitude as an additional unknown and solves loads and displacements simultaneously. Therefore, another quantity must be used to measure the progress of the solution. ABAQUS uses the arc length along the static equilibrium path in load displacement domain. This approach provides solutions regardless of whether the response is stable or unstable. If the Riks step is a continuation of a previous history, any loads that exist at the beginning of the step are treated as dead loads with constant magnitude. A load whose magnitude is defined in the Riks step is referred to as a reference load. All prescribed loads are ramped from the initial (dead load) value to the reference values specified. ABAQUS uses Newton's method to solve the nonlinear equilibrium equations. The Riks procedure uses very small extrapolation of the strain increment. Modelers can provide an initial increment in arc length along the static equilibrium path when defining the step. After that, ABAQUS computes subsequent steps automatically. Since the loading magnitude is part of the solution, modelers need a method to specify when the step is completed. It is common that one can specify a maximum displacement value at a specified degree of freedom. The step will terminate once the maximum value is reached. Otherwise, the analysis will continue until the maximum number of increments specified in the step definition is reached.

The Riks method works well with structures having a smooth equilibrium path in load-displacement domain. The Riks method can be used to solve post-buckling problems, both with stable and unstable post-buckling behavior. In this way, the Riks method can be

used to perform post-buckling analyses of structures that show linear behavior prior to (bifurcation) buckling. When performing a load-displacement analysis using the Riks method, important nonlinear effects can be included. Imperfections based on linear buckling modes can be also included in the analysis of structures using the Riks method. It should be noted that the Riks method cannot obtain a solution at a given load or displacement value since these are treated as unknowns. Termination of the analysis using the Riks method occurs at the first solution that satisfies the step termination criterion. To obtain solutions at exact values of load or displacement, the analysis must be restarted at the desired point in the step and a new, non-Riks step must be defined. Since the subsequent step is a continuation of the Riks analysis, the load magnitude in that step must be given appropriately so that the step begins with the loading continuing to increase or decrease according to its behavior at the point of restart.

Initial values of stresses such as residual stresses can be inserted in the analysis using the Riks method. Also, boundary conditions can be applied to any of the displacement or rotation degrees of freedom (six degrees of freedom).Nonlinear material models that describe mechanical behavior of metal structures can be incorporated in the analysis using the Riks method.

3.6.5 Flowchart for finite element analysis

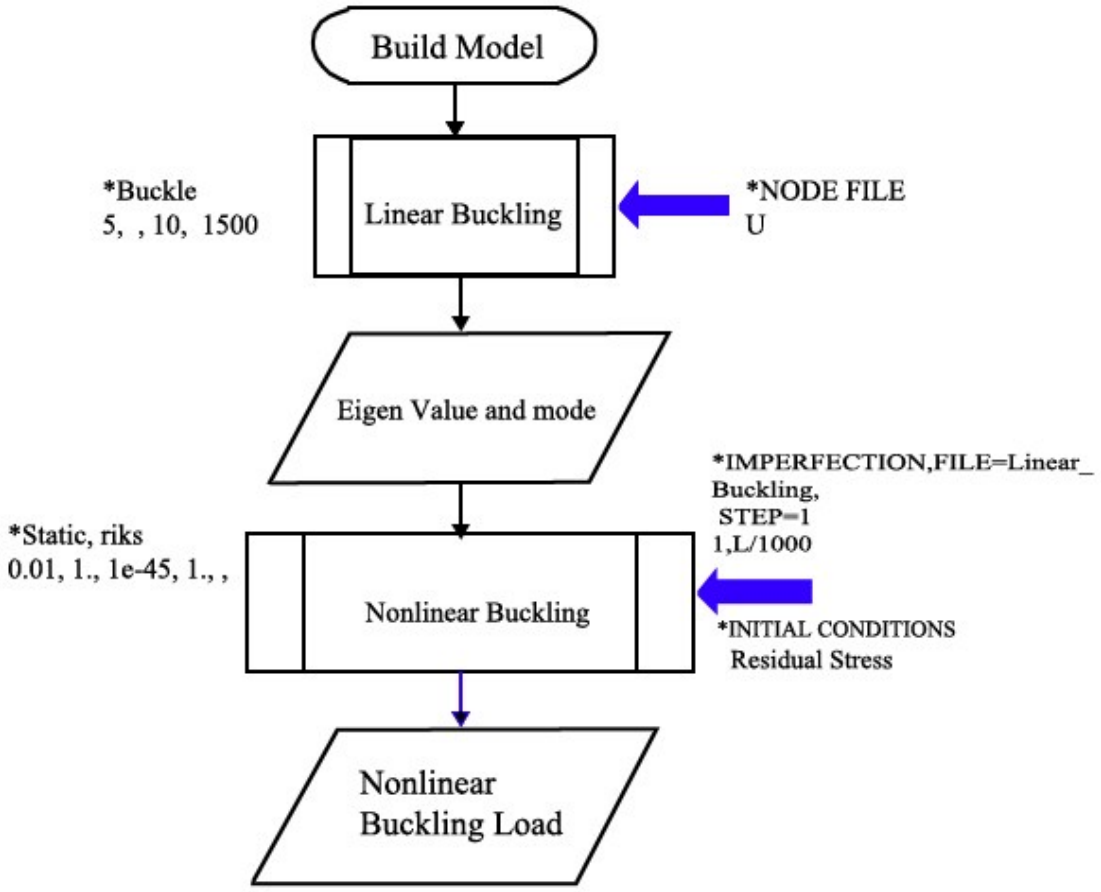

Figure 3-6: Flowchart for the finite element analysis

3.7 Solution

All elastic-plastic buckling GMNIA are load-controlled. A force with specified magnitude was applied at the top of the column. The Arc-Length method was selected to solve the non-linear equilibrium iterations. The Arc-Length method was selected in preference to the conventional Newton-Raphson method as the former is able to describe the decreasing load-deflection curve beyond the maximum load whereas the latter will abort the solution when the maximum resistance has been reached. The load was divided into four load steps which in turn were further divided into sub steps or load increments. For each load-increment, a number of equilibrium iterations were performed to arrive at a converged solution. The ultimate strength or flexural buckling resistance of the column ($N_{ult;FEM}$) was identified as the maximum load on the load-deflection curve. The elastic

buckling load ($N_{cr;FEM}$) is obtained from a linear buckling analysis (LBA) using the Subspace extraction method of eigenvalues.

3.8 Plotting Results in Buckling Curve

For each column configuration for which the ultimate resistance is evaluated through non-linear finite element analyses, the reduction factor is obtained by normalizing the ultimate load against the squash load of the cross-section ($N_{pl;FEM}$).

$$\chi_{FEM} = \frac{N_{ult;FEM}}{N_{pl;FEM}} \tag{3.3}$$

where the squash load of the cross-section is computed according to:

$$N_{pl;\mathrm{FEM}} = Af_y \tag{3.4}$$

where A is the cross-sectional area of the element and f_y is the yield stress. The factor χ_{FEM} is labeled as the 'Numerical' resistance for comparison with the theoretical resistance χ. The relative slenderness of the column can be computed by taking the square root of the ratio between the squash load of the cross-section and the elastic buckling load evaluated from a linear buckling analysis:

$$\bar{\lambda}_{FEM} = \sqrt{\frac{N_{pl:FEM}}{N_{cr;FEM}}} \tag{3.5}$$

Then plotting the result by considering reduction factor as the y-axis and the relative slenderness as the x-axis. Compare the results with existing buckling curves given in EN 1993-1-1 [8].

CHAPTER 4 RESULT AND DISCUSSION

4.1 Validation

Key and Hancock [7] experiment were chosen for the validation of finite element analysis.

4.1.1 Key and Hancock's experiments

A series of carefully conducted column experiments have been reported by Key and Hancock [7] on Australian produced cold-formed square hollow sections (SHS). Tests were conducted on tube size: 203x203x6.3, with slenderness ratios L/r in the range of 15-100. The width to thickness ratios of these tubes are quite low (<38) and so preclude the occurrence of local buckling within the elastic range. Measurements were made of yield stress around the tube perimeter, residual stress distribution, stub column and initial out-of-straightness.

The pin ended test columns were loaded concentrically and axial shortening, Δ, were recorded at increments up to and past the maximum load into the post-ultimate unloading range. The information presented by Key and Hancock [7] thus provides invaluable data for comparison with current theoretical work. The longitudinal residual stress in cold-formed SHS consists of two components: the membrane component and the bending or the through thickness component. As shown in Figure 4-1a the membrane component is only of the order of 30 MPa tensile at the center of each face and 30 MPa compressive near the tube corners and has little influence on the column behavior. Key and Hancock [7] showed that the average maximum bending residual stress is approximately $\pm$140 MPa compared with a yield stress of about 400 MPa and Young's modulus of 200 GPa. The bending residual stress distribution shown in Figure 4-1 b is used for cold-formed column investigated in this section.

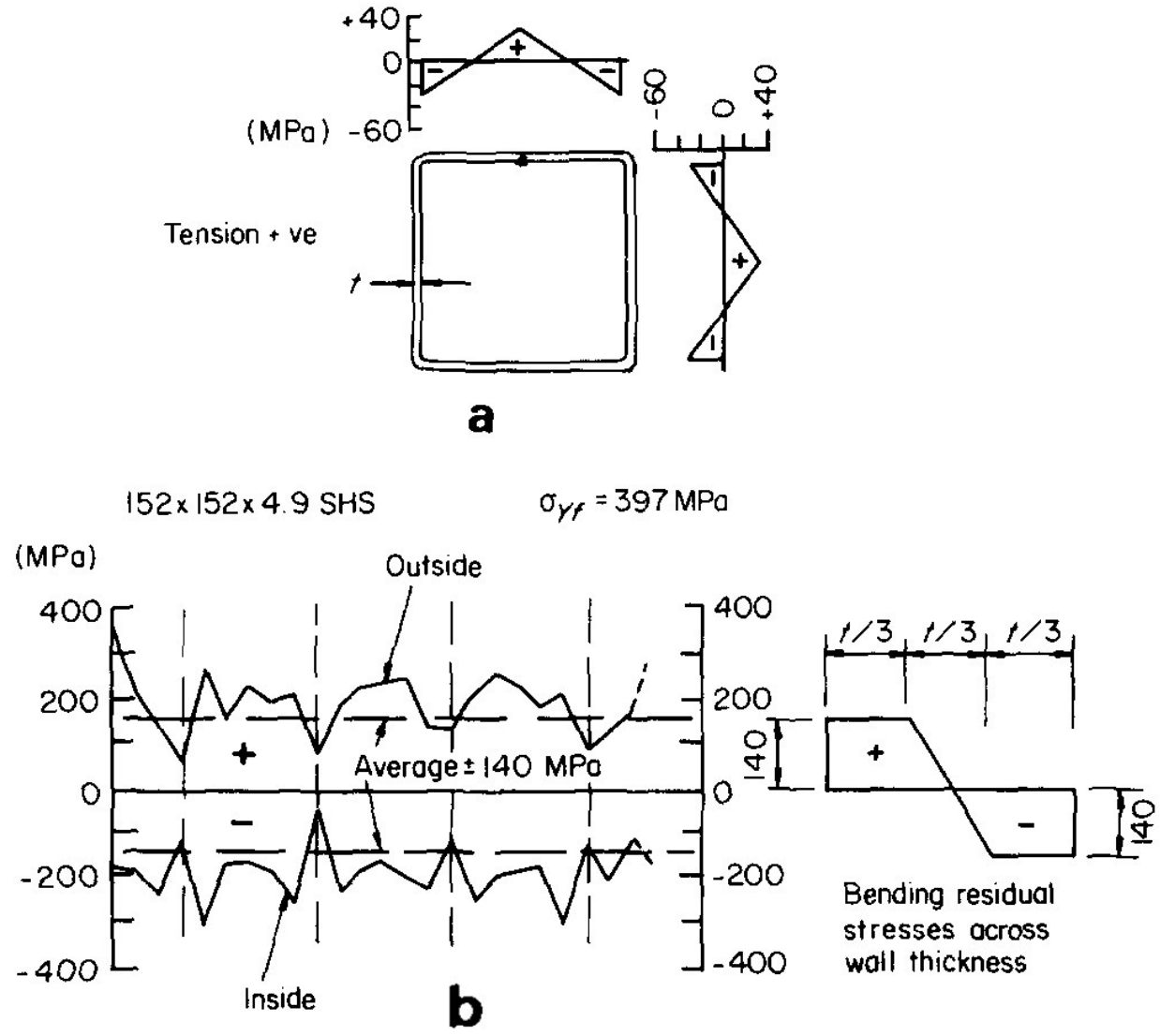

Figure 4-1: Residual stress distribution in cold-formed square hollow sections: (a) measured average membrane residual stress distribution; (b) measured longitudinal stresses around tube [7].

For the purpose of the present numerical study, the tube size 203x203x6.3 SHS was selected. From the available three tested with column length the one that has maximum length was chosen because of more sensitive to buckling failure. The buckling load in the linear buckling analysis was found to be 1.02798×10^6 N and was observed at mode 1 at which the flexural buckling occurs.

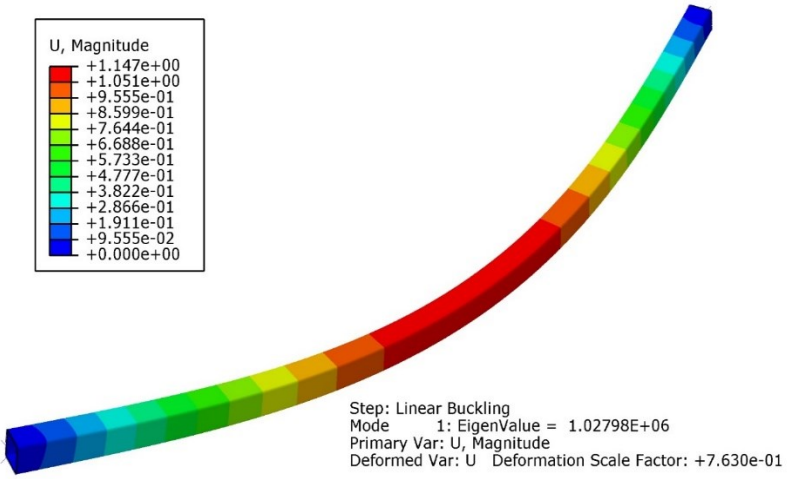

Figure 4-2: shows mode 1 of the buckled mode shapes of the column.

Figure 4-3 shows the load and the axial shortening relations for concentrically loaded columns having slenderness ratios L/r of 95.7, either with or without residual stress.

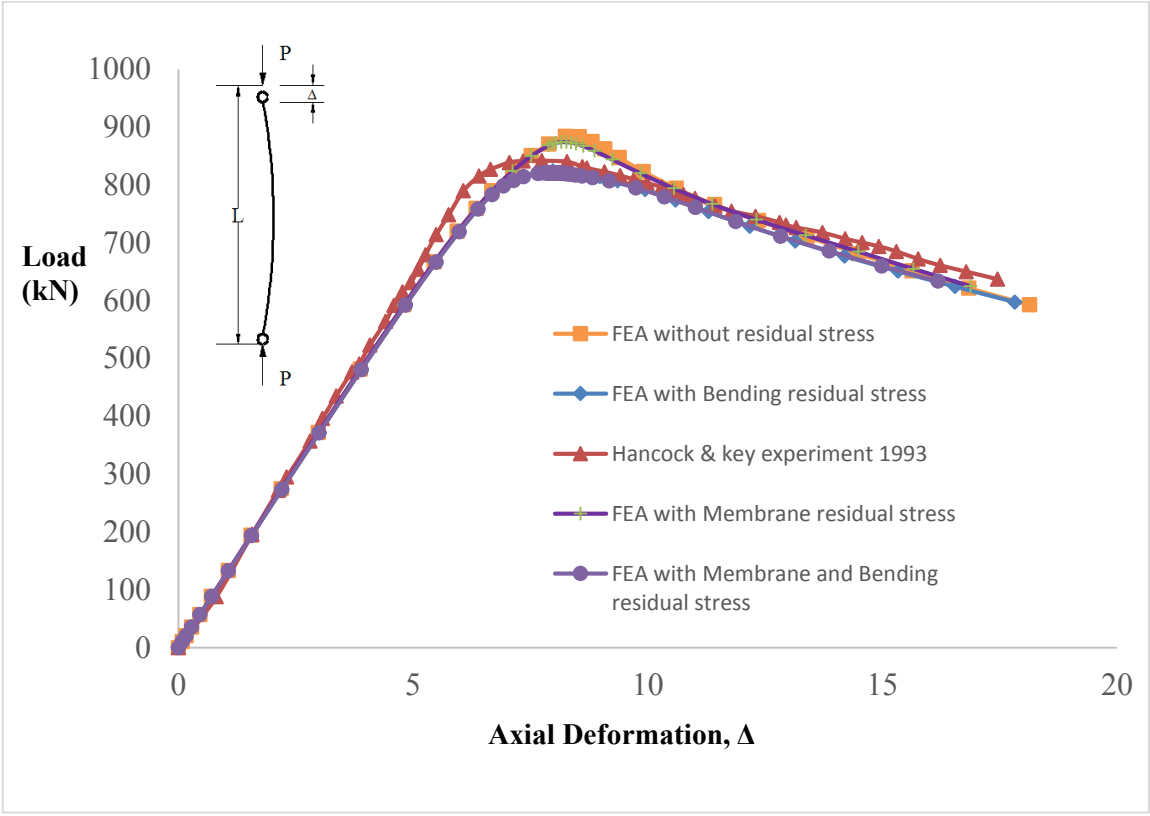

Figure 4-3: Comparison of Numerical and Experimental axial load-shortening curves for 203x203x6.3 SHS cold-formed column with L/r= 95.7.

It can be seen that the numerical curves closely follow the test result. The presence of residual stress reduces the ultimate loads of column. Table Shows the Comparison numerical and experimental maximum column loads.

Table 4-1: Comparison of Numerical and Experimental maximum loads for cold-formed SHS columns.

Experiment and Numerical Results	Maximum load (kN)	Convergence (%)
Hancock & key experiment 1993 (1)	841.55	0.00
FEA without residual stress (2)	883.68	4.77
FEA with Membrane residual stress (3)	874.00	3.71
FEA with Bending residual stress (4)	824.16	-2.11
FEA with Membrane and Bending residual stress (5)	820.96	-2.51

The difference in predicted ultimate load between combinations (1) and (2) is approximately 4.77%, which indicates that a model without residual stress overestimates column maximum load. The difference in predicted ultimate load between combinations (2) and (3) is approximately 1.06%, which indicates that membrane residual stresses component had a negligible influence on the section behavior. The difference in ultimate load of approximately 2.11% between cases (1) and (4), and 2.51% between cases (1) and (5) suggests the bending component of residual stress has a larger influence on column buckling loads.

4.1.2 Convergence study on the non-linear buckling analysis

In finite element analysis, to obtain accurate results, the mesh refinement levels must be good enough. In this work, the 8-node linear brick, reduced integration (C3D8R) element was used. A convergence study based on nonlinear buckling was conducted in this work. The study was conducted on linear element type mesh with an element size of 10 mm, 20 mm, 30 mm and 40 mm along the length. The buckling load for a 10 mm element size linear element type mesh was 829.31 kN, the buckling load for a 20 mm element size linear element type mesh was 820.96 kN, and the buckling load for a 30 mm element size linear element type mesh was 809.19 kN, while the buckling load for a 40 mm element size linear element type mesh was 802.74 kN. It can be clearly seen that the results are converging.

Though the results from each element size would be similar, the 10 mm element size would be better. However, in this thesis, the 20 mm element size was used due to computational time.

4.1.3 Comparison with buckling curves

Figure 4-4 shows the FEA and Experiment results and their comparisons with all five buckling curves. The proposed column is derived from the Perry equation that is adopted in EN 1993-1-1 [8].

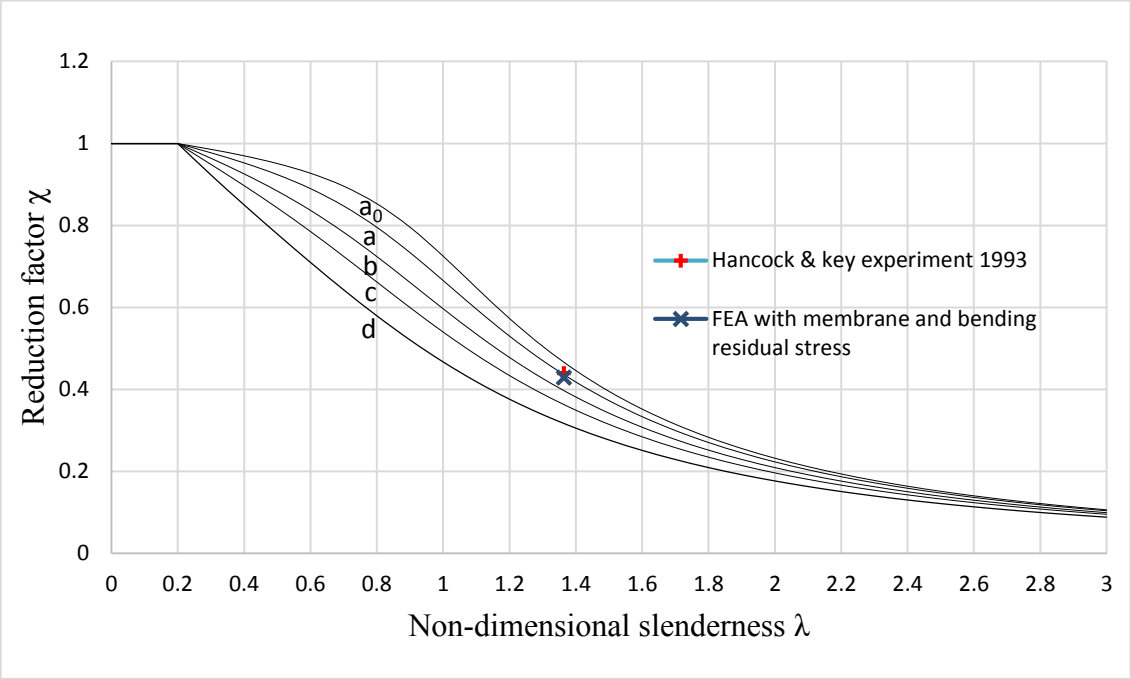

Figure 4-4: Comparison of Numerical and experimental maximum column loads with all five buckling curves.

In Figure 4-4 the Numerical and experimental loads are plotted in the buckling curve diagram. There is a reasonable fit to buckling curve "a".

4.2 Material Behavior

Annex C of EN 1993-1-5 [9] recommends the use of one of the following three material behavior models when performing plated finite element analysis:

a) elastic–plastic without strain hardening

b) elastic–plastic with a nominal plateau slope of 1 MPa

c) elastic–plastic with a strain hardening slope of E/100

From Annex C of EN 1993-1-5 [9] recommendation material behavior three of listed above were used. First linear buckling analysis was done before the nonlinear analysis. The critical load from the linear eigenvalue analysis (LBA) of the numerical model does not necessarily have to be the same as the Euler buckling formula Eq. (2.1). This can be due to the compressive residual stress and small changes in bending stiffness originating from the non-uniform material distribution. Both results were compared, and their difference was lower than 1.5%. For this study the linear eigenvalue analysis (LBA) of the numerical model was used.

For the purpose of the material behavior study, the tube size 340x100x10 RHS subjected to major axis buckling was selected. The buckling load of 340x100x10 RHS with the three material model results were compared for the column length of 6m and 10.85 m, with residual stress.

Table 4-2: Comparison of buckling load for elastic–plastic without strain hardening, with a nominal plateau slope of 1 MPa and with a strain hardening slope of E/100(6 m).

Steel Grade	elastic-plastic without strain hardening	elastic-plastic with a nominal plateau slope of 1 Mpa(kN)	elastic-plastic with a strain hardening slope of E/100(kN)
S275	2059.90	2060.68 0.04%	2068.78 0.43%
S355	2605.25	2606.15 0.01%	2612.74 0.29%
S420	3024.63	3025.84 0.04%	3034.94 0.34%
S460	3270.16	3271.24 0.03%	3085.08 0.34%

Table 4-3: Comparison of buckling load for elastic–plastic without strain hardening, with a nominal plateau slope of 1 MPa and with a strain hardening slope of E/100(10.85 m).

Steel Grade	elastic-plastic without strain hardening	elastic-plastic with a nominal plateau slope of 1 Mpa(kN)	elastic-plastic with a strain hardening slope of E/100(kN)
S275	1386.35	1386.37 (0.001%)	1388.12 (0.126%)
S355	1532.79	1532.79 (0.000%)	1534.24 (0.094%)
S420	1603.95	1603.96 (0.000%)	1605.04 (0.068%)
S460	1635.26	1635.27 (0.000%)	1636.30 (0.063%)

It can be seen that the buckling load of the results are very close to each other. The elastic-plastic without strain hardening and elastic-plastic with a nominal plateau slope of 1 Mpa are almost have the same buckling loads. Elastic-plastic with a strain hardening slope of E/100 gives a little higher buckling load but did not significantly affect the results and the effect of incorporating the ultimate strength was also relatively small. When the column length increases, the effect of material behavior became less due to the fact that geometric failure dominates rather than material failure.

Elastic-plastic without strain hardening is a little conservative approach. Therefore, Elastic-plastic without strain hardening was used for buckling curves analysis.

4.3 Residual Stress

The commonly used residual stresses based on ECCS [6] recommendations were adopted and also introduced in the numerical model of this investigation due to its simplicity and commonly used. The effect of incorporating residual stress was carefully investigated. The tube size 340x100x10 RHS subjected to minor axis buckling was selected. The buckling load of 340x100x10 RHS with the residual and without residual stress compared for the 3m, 4m and 5m column heights.

Table 4-4: Comparison of Buckling load of columns with and without residual stress.

Column height	Steel Grade	FEA without residual stress(kN)	FEA with residual stress(kN)	Difference (%)
3 m	S235	1672.06	1607.65	4.01
	S275	1895.55	1834.67	3.32
	S355	2295.28	2256.60	1.71
	S420	2527.29	2488.55	1.56
	S460	2628.66	2589.10	1.53
4 m	S235	1365.92	1321.04	3.40
	S275	1454.27	1446.17	0.56
	S355	1585.73	1578.65	0.45
	S420	1638.50	1634.90	0.22
	S460	1655.87	1654.55	0.08
5 m	S235	1003.73	991.94	1.19
	S275	1035.35	1029.83	0.54
	S355	1076.85	1073.25	0.34
	S420	1095.23	1093.14	0.19
	S460	1098.37	1097.63	0.07

As we see in the Table 4-4 the residual stress effect decreases as the strength of steel increase. ECCS [6] residual stress constant for steel grade S235 to S460 because of this the effect of residual stress were lower as increasing of steel grade. In addition, the Effect of residual stresses were investigated through the heights of columns and the effect were reduced as the height of the columns increases. As the column length increases, the effect of residual stress became less due to the fact that geometric failure dominates rather than material failure.

4.4 Buckling Curves for Hollow Sections

In order to propose a design buckling curve, a pin-ended column with the different cross-sectional area and length under axial compression around both the minor and major axis were calculated using ABAQUS. For each column, the initial geometric imperfection and residual stresses are taken as exactly as mentioned earlier. Linear and Non-linear analysis were carried out to determine the buckling capacity of columns. For the purpose of the

present numerical study, different tube size with varying height to width (h/b) ratio of a cross section were selected.

a) **340x100x10mm** RHS

The ratio of height to width (h/b) of a cross section is 3.4, there is high difference between the height to width ratio. The two axis have a different radius of gyration, for comparison purpose the author took different heights for each axis but with the same slenderness ratio. All steel grade were considered in the numerical analysis.

Major axis

Column that has 10.85 m long was selected with slenderness ratio of 96 subjected to strong axis buckling.

Table 4-5: Reduction factor and non-dimensional slenderness ratio for 340x100x10mm subjected to major axis buckling(10.85 m).

	S235	S275	S355	S420	S460
$N_{ult;FEM}$ (kN)	1275.39	1386.35	1532.77	1603.95	1635.26
$N_{pl;FEM}$ (kN)	1948.78	2280.49	2943.91	3482.93	3814.64
$N_{cr;FEM}$ (kN)	1847.91	1847.91	1847.91	1847.91	1847.91
χ_{FEM}	0.65	0.61	0.52	0.46	0.43
$\bar{\lambda}_{FEM}$	1.03	1.11	1.26	1.37	1.44

Minor axis

Column that has 4m long was selected with slenderness ratio of 96 subjected to weak axis buckling.

Table 4-6: Reduction factor and non-dimensional slenderness ratio for 340x100x10mm subjected to major axis buckling(4 m).

	S235	S275	S355	S420	S460
$N_{ult;FEM}$ (kN)	1321.04	1446.17	1578.65	1634.90	1654.55
$N_{pl;FEM}$ (kN)	1948.78	2280.49	2943.91	3482.93	3814.64
$N_{cr;FEM}$ (kN)	1821.03	1821.03	1821.03	1821.03	1821.03

χ_{FEM}	0.68	0.63	0.54	0.47	0.43
$\bar{\lambda}_{FEM}$	1.03	1.12	1.27	1.38	1.45

The buckling curves were investigated after drew it on existing European buckling curves.

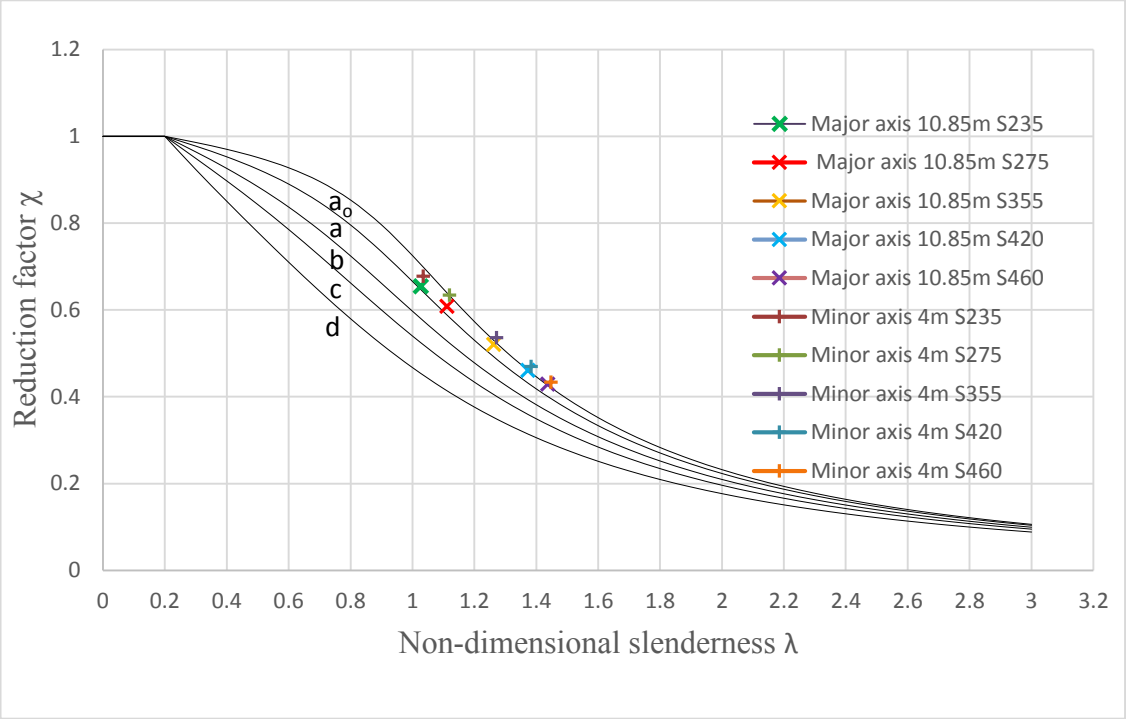

Table 4-7: FEA results of the 340x100x10mm columns and their comparison with all five buckling curves.

The plotted curves fully agree with the recommended buckling curves in Eurocode 3 [8] for hot finished hollow sections. In addition to that the minor axis buckling have high buckling curves compared to the major axis of the same slenderness ratio. Major axis buckling gives curve "a" for S235 to S355 and "a_0" for S420 to S460. Minor axis buckling gave curve "a" for S235 and "a_0" for S275 to S460.

Due to computational time it is difficult to run multiple analysis, so that to see the replicability of the results additional column lengths that is 8m, 12.5m additional to the 10.85m length for major axis buckling and 3m, 5m additional to the 4m length for minor axis buckling were plotted in figure below.

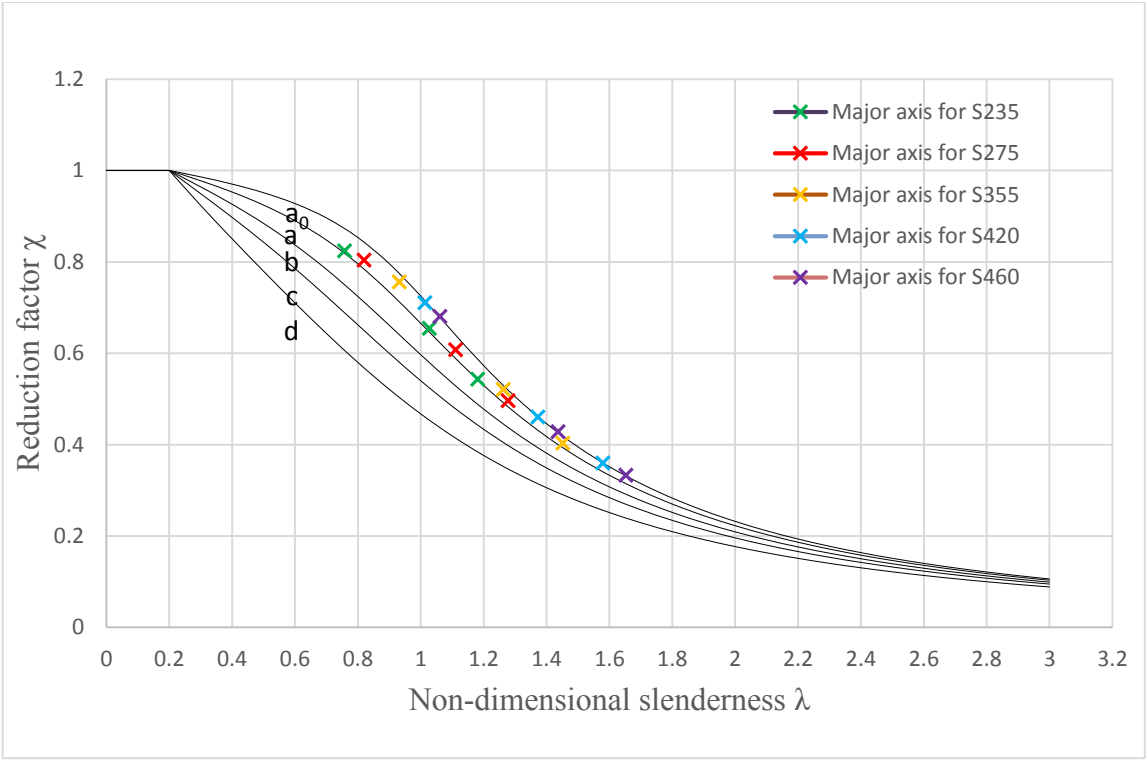

(a)

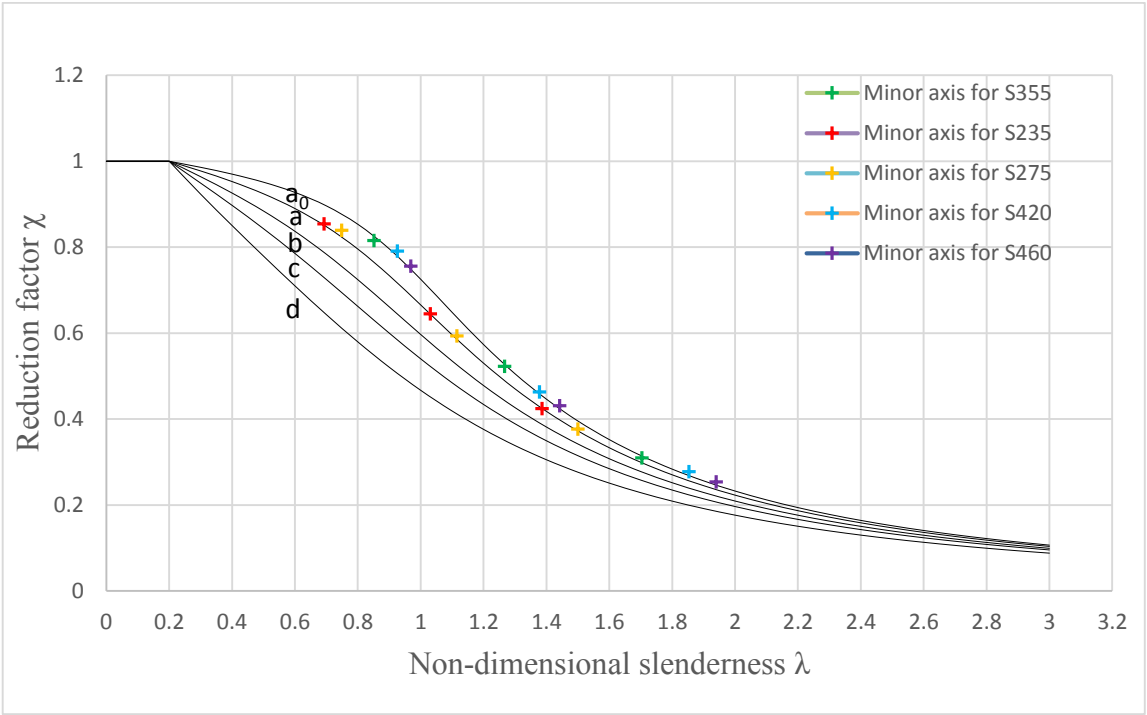

(b)

Figure 4-5: FEA results of the 340x100x10mm columns and their comparison with all five buckling curves; (a) major axis, (b) minor axis.

The plotted curves agree with the previous draw one for the same section with different length. Major axis buckling gives curve "a" for S235 to S355 and "a_0" for S420 to S460. Minor axis buckling gave curve "a" for S235 and "a_0" for S275 to S460.

b) 200x100x10mm RHS

The ratio of height to width (h/b) of a cross section is 2.0, there is medium difference between the height to width ratio. The two axis have a different radius of gyration, for comparison purpose the author took different heights for each axis but with the same slenderness ratio. All steel grade were considered in the numerical analysis.

Major axis

Column that has 6.68 m long was selected with slenderness ratio of 96 subjected to strong axis buckling.

Table 4-8: Reduction factor and non-dimensional slenderness ratio for 200x100x10mm subjected to major axis buckling(6.68 m).

	S235	S275	S355	S420	S460
$N_{ult;FEM}$ (kN)	832.04	889.88	958.04	1024.40	1081.78
$N_{pl;FEM}$ (kN)	1290.78	1510.49	1949.91	2306.93	2526.64
$N_{cr;FEM}$ (kN)	1221.83	1221.83	1221.83	1221.83	1221.83
χ_{FEM}	0.64	0.59	0.49	0.44	0.42
$\bar{\lambda}_{FEM}$	1.03	1.11	1.26	1.37	1.44

Minor axis

Column that has 3.82 m long was selected with slenderness ratio of 96 subjected to weak axis buckling.

Table 4-9: Reduction factor and non-dimensional slenderness ratio for 200x100x10mm subjected to major axis buckling(3.82 m).

	S235	S275	S355	S420	S460
$N_{ult;FEM}$ (kN)	823.47	920.26	1033.52	1079.97	1096.68
$N_{pl;FEM}$ (kN)	1290.79	1510.49	1949.91	2306.93	2526.64

$N_{cr;FEM}$ (kN)	1213.56	1213.56	1213.56	1213.56	1213.56
χ_{FEM}	0.64	0.61	0.53	0.47	0.43
$\overline{\lambda}_{FEM}$	1.03	1.12	1.27	1.38	1.44

The buckling curves were investigated after drew it on existing European buckling curves.

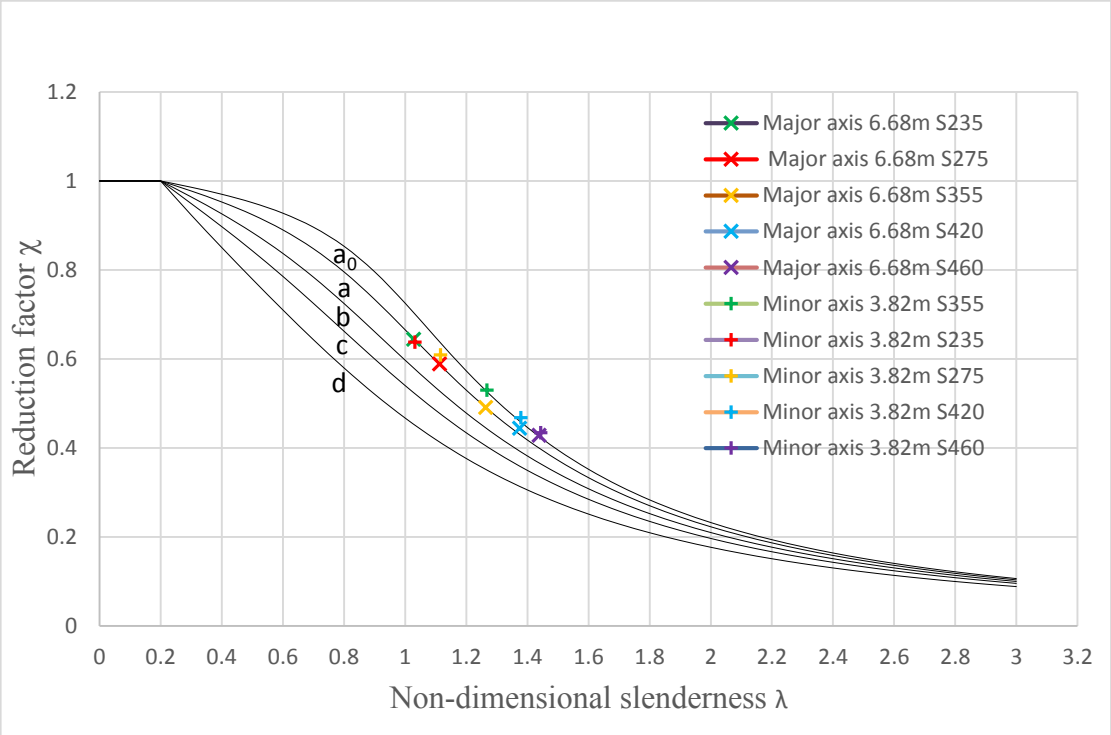

Figure 4-6: FEA results of the 200x100x10mm columns and their comparison with all five buckling curves.

The plotted curves fully agree with the recommended buckling curves in Eurocode 3 [8] for hot finished hollow sections. In addition to that the minor axis buckling have high buckling curves compared to major axis of the same slenderness ratio. Major axis buckling gives curve "a" for S235 to S420 and "a_0" for S460. Minor axis buckling gives curve "a" for S235 to S275 and "a_0" for S355 to S460.

To see the replicability of the results additional column lengths that is 4m, 9m additional to the 6.68m length for major axis buckling and 2.9m, 5m additional to the 3m length for minor axis buckling were plotted in figure below.

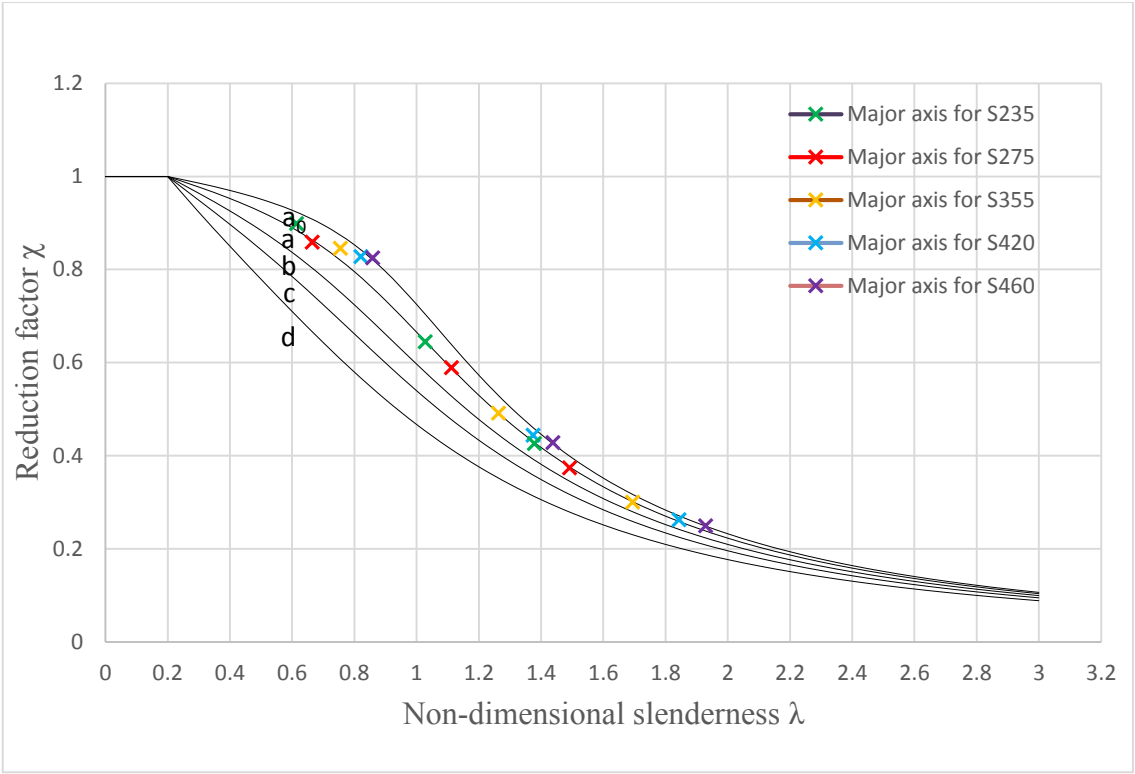

(a)

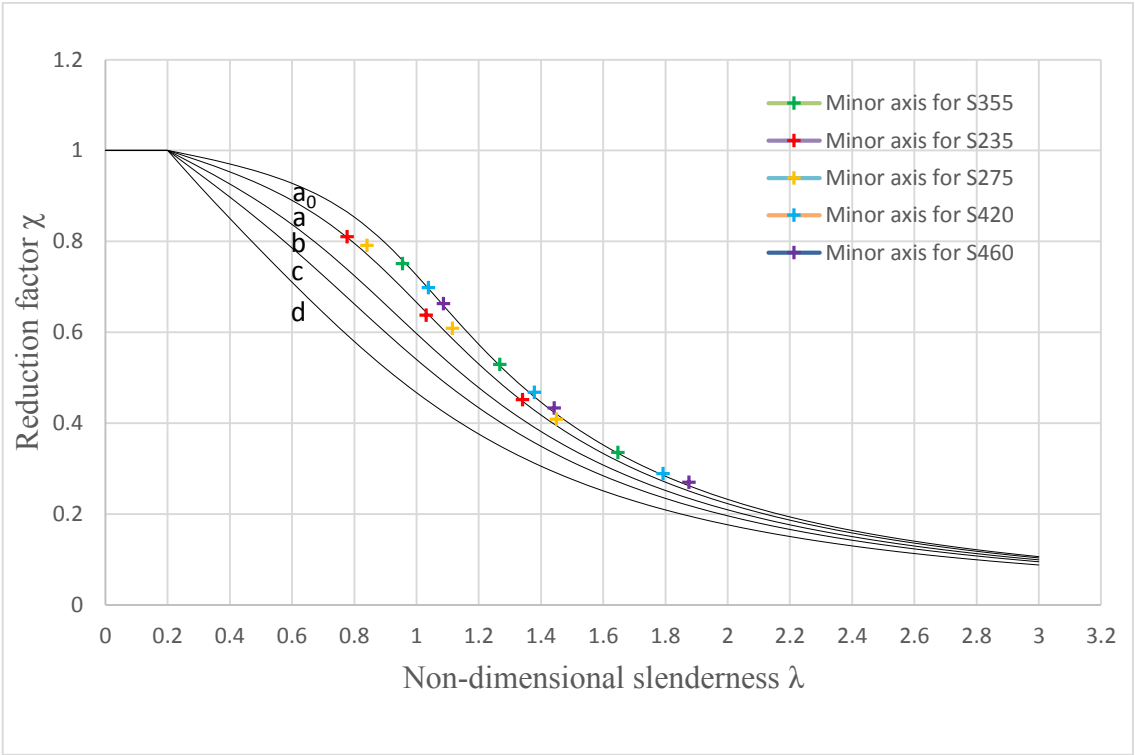

(b)

Figure 4-7: FEA results of the 200x100x10mm columns and their comparison with all five buckling curves; (a) major axis, (b) minor axis.

The plotted curves agree with the previous draw one for the same section with different length. Major axis buckling gives curve "a" for S235 to S420 and "a_0" for S460. Minor axis buckling gives curve "a" for S235 to S275 and "a_0" for S355 to S460.

c) 150x100x10mm RHS

The ratio of height to width (h/b) of a cross section is 1.5, there is low difference between the height to width ratio. The two axis have a different radius of gyration, for comparison purpose the author took different heights for each axis but with the same slenderness ratio. All steel grade were considered in the numerical analysis.

Major axis

Column that has 5.13 m long was selected with slenderness ratio of 96 subjected to strong axis buckling.

Table 4-10: Reduction factor and non-dimensional slenderness ratio for 150x100x10mm subjected to major axis buckling (5.13 m).

	S235	S275	S355	S420	S460
$N_{ult;FEM}$ (kN)	677.98	725.01	781.81	842.07	867.15
$N_{pl;FEM}$ (kN)	1055.78	1235.49	1594.91	1886.93	2066.64
$N_{cr;FEM}$ (kN)	997.51	997.51	997.51	997.51	997.51
χ_{FEM}	0.64	0.59	0.49	0.45	0.42
$\overline{\lambda}_{FEM}$	1.03	1.11	1.26	1.38	1.44

Minor axis

Column that has 3.69 m long was selected with slenderness ratio of 96 subjected to weak axis buckling.

Table 4-11: Reduction factor and non-dimensional slenderness ratio for 150x100x10mm subjected to minor axis buckling (3.695 m).

	S235	S275	S355	S420	S460
$N_{ult;FEM}$ (kN)	681.28	733.50	834.15	874.08	891.10
$N_{pl;FEM}$ (kN)	1055.78	1235.49	1594.91	1886.93	2066.64
$N_{cr;FEM}$ (kN)	993.52	993.52	993.52	993.52	993.52

χ_{FEM}	0.65	0.59	0.52	0.46	0.43
$\bar{\lambda}_{FEM}$	1.03	1.12	1.27	1.38	1.44

The buckling curves were investigated after drew it on existing European buckling curves.

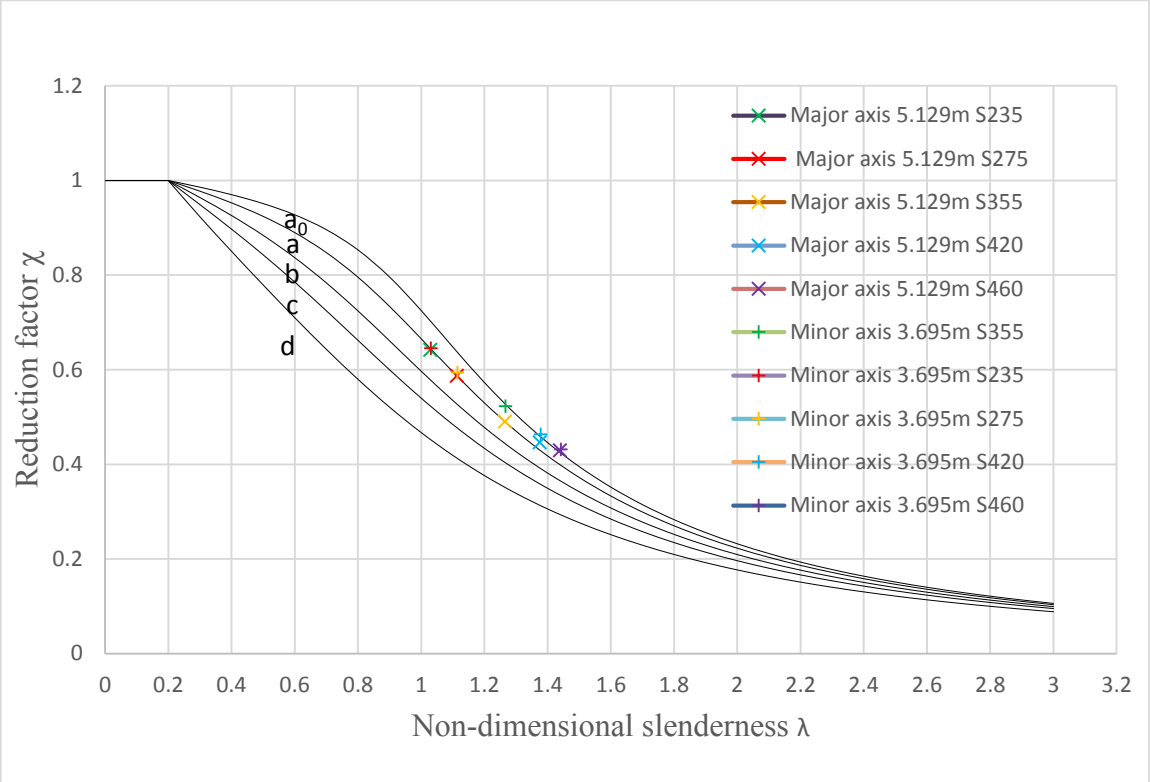

Figure 4-8: FEA results of the 150x100x10mm columns and their comparison with all five buckling curves.

The plotted curves fully agree with the recommended buckling curves in Eurocode 3 [8] for hot finished hollow sections. In addition to that the minor axis buckling has high buckling curves compared to the major axis of the same slenderness ratio. Major axis buckling gives curve "a" for S235 to S420 and "a_0" for S460. Minor axis buckling gives curve "a" for S235 to S275, S355 nearly to "a_0" and "a_0" for S420 to S460.

To see the replicability of the results additional column lengths that is 3m, 6.5m additional to the 5.129m length for major axis buckling and 2.5m, 5m additional to the 3.695m length for minor axis buckling were plotted in figure below.

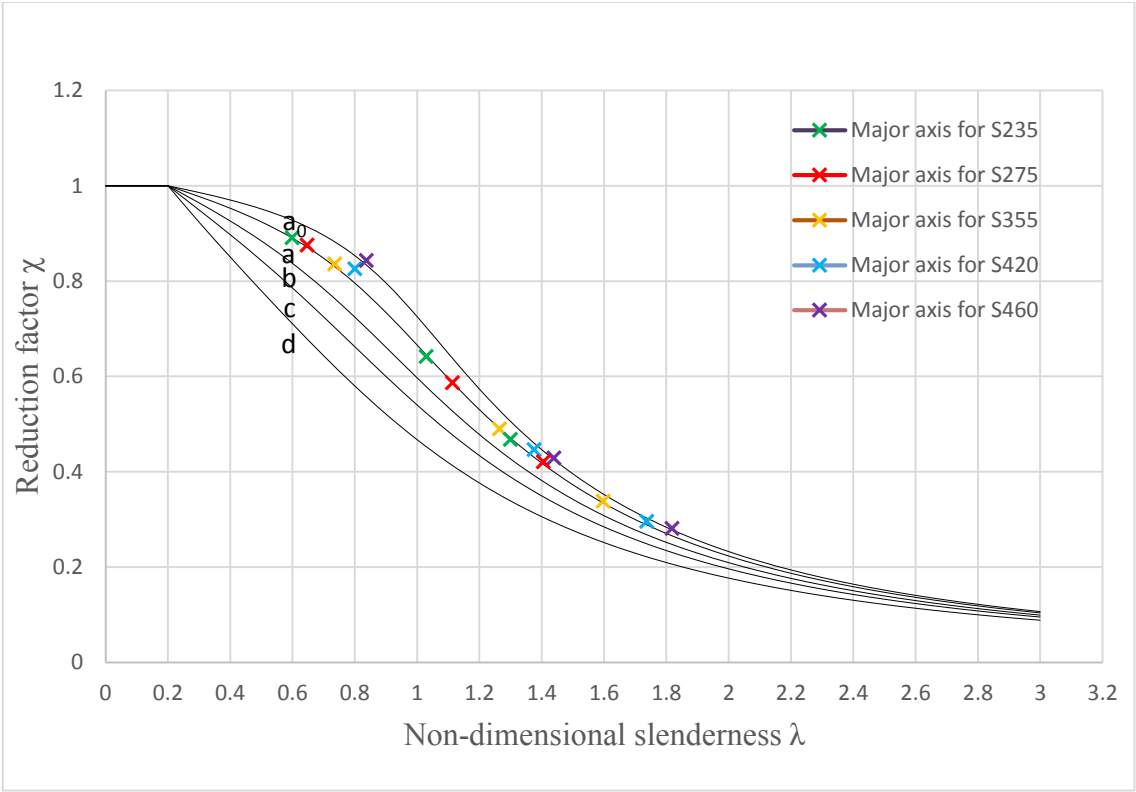

(a)

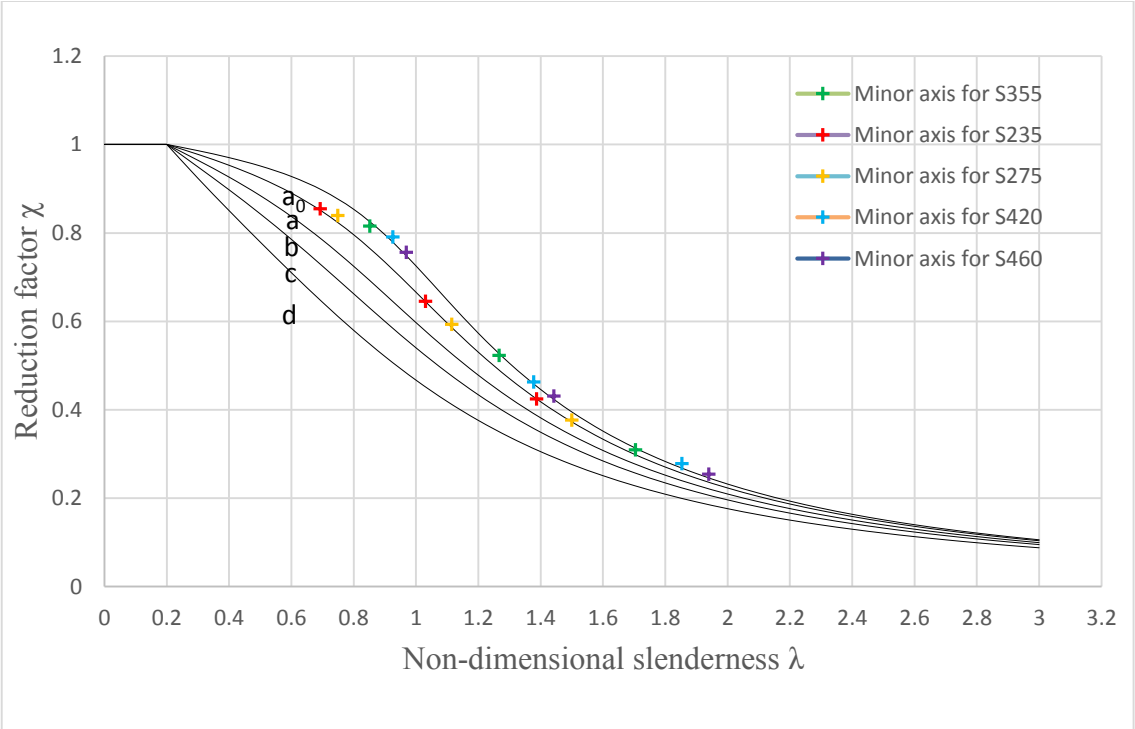

(b)

Figure 4-9: FEA results of the 150x100x10mm columns and their comparison with all five buckling curves; (a) major axis, (b) minor axis.

The plotted curves agree with the previous draw one for the same section with different length. Major axis buckling gives curve "a" for S235 to S420 and "a_0" for S460. Minor axis buckling gives curve "a" for S235 to S275, S355 nearly to "a_0" and "a_0" for S420 to S460.

d) 100x100x10mm RHS

The ratio of height to width (h/b) of a cross section is 1.0. The section has the same radius of gyration on both axis, for comparison purpose the author took 3.5 m long column with the same slenderness ratio as the previous models. All steel grade were considered in the numerical analysis.

Table 4-12: Reduction factor and non-dimensional slenderness ratio for 100x100x10mm subjected to major axis buckling (3.5 m).

	S235	S275	S355	S420	S460
$N_{ult;FEM}$ (kN)	524.79	560.90	615.48	649.22	663.27
$N_{pl;FEM}$ (kN)	820.78	960.49	1239.91	1466.93	1606.64
$N_{cr;FEM}$ (kN)	772.12	772.12	772.12	772.12	772.12
χ_{FEM}	0.64	0.58	0.50	0.44	0.41
$\bar{\lambda}_{FEM}$	1.03	1.12	1.27	1.38	1.44

The buckling curves were investigated after drew it on existing European buckling curves.

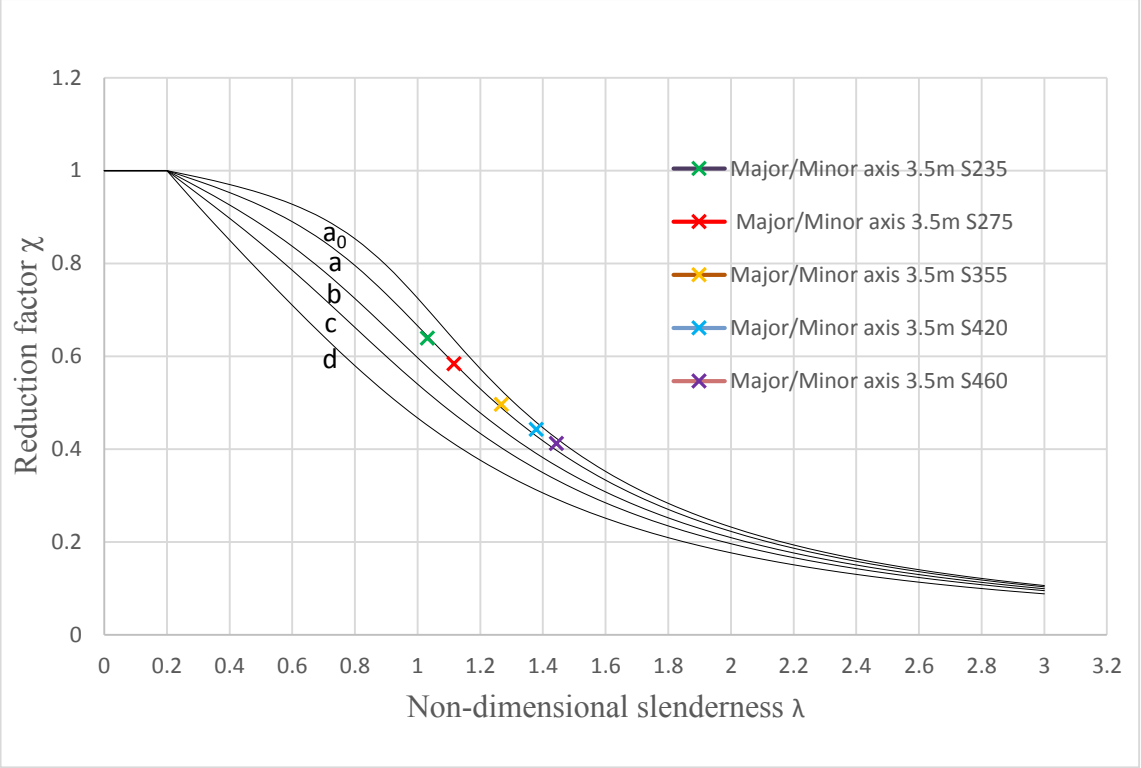

Figure 4-10: FEA results of the 100x100x10mm column and their comparison with all five buckling curves.

The plotted curves fully agree with the recommended buckling curves in Eurocode 3 [8] for hot finished hollow sections. Major/Minor axis buckling gives curve "a" for S235 to S420 and "a_0" for S460.

To see the replicability of the results additional column lengths that is 2.5m, 5m additional to the 3.5m length for major/minor axis buckling were plotted in figure below.

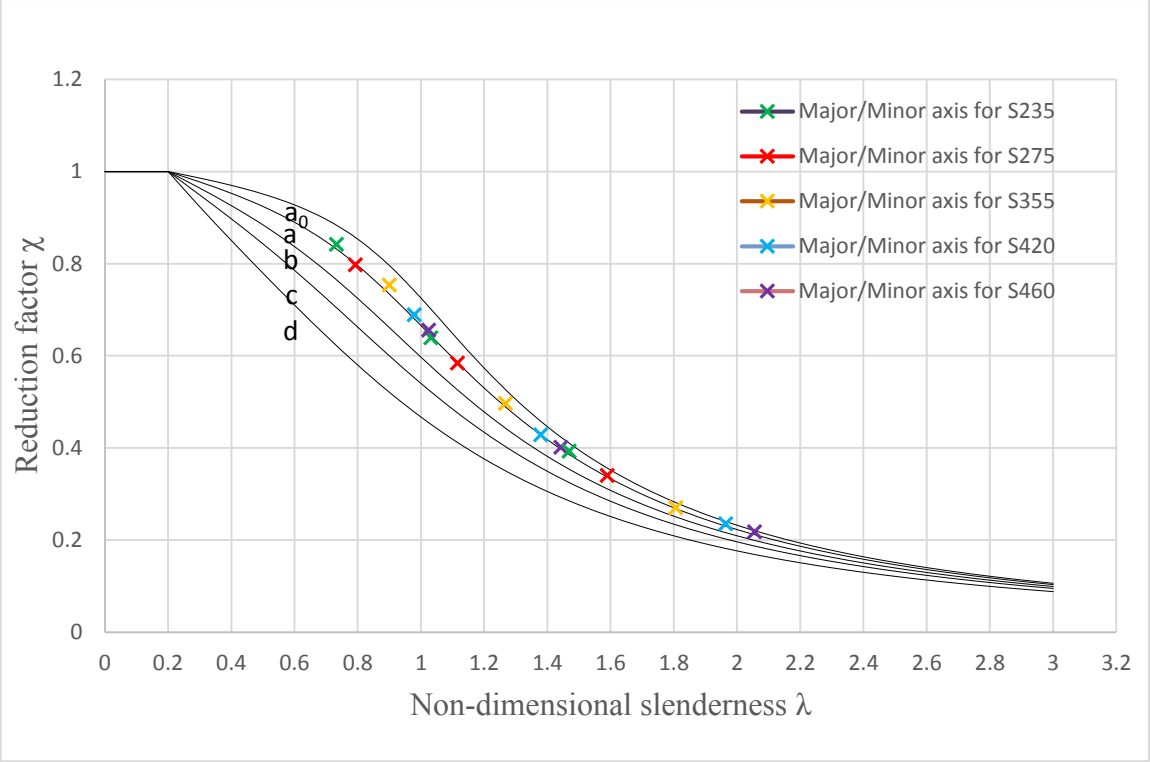

Figure 4-11: FEA results of the 100x100x10mm column and their comparison with all five buckling curves.

The plotted curves agree with the previous draw one for the same section with different length. Major/Minor axis buckling gives curve "a" for S235 to S420 and "a_0" for S460.

Rectangular sections have high buckling curve than that of square sections with the same slenderness ratio subjected to weak axis buckling. The minor axis has high buckling curve when the ratio of height to width high. When the ratio height to width of a cross section (H/B) greater than 3, minor axis buckling gives "a_0" for Steel Grade S355 to S460. The major axis buckling has the same buckling curves given in Eurocode 3 [8].

CHAPTER 5 CONCLUSIONS AND RECOMMENDATIONS

5.1 Conclusions

It has been shown that it is possible to simulate the European buckling curves using non-linear finite element modeling of flexural column buckling using solid elements. A number of columns have been analyzed by advanced geometric and material non-linear analysis with imperfections (GMNIA) using different magnitudes of characteristic yield stress, material stress-strain relationships, and equivalent imperfections and/or residual stresses for standard hot-rolled profiles.

From the results obtained in this work, the following conclusions are drawn:

1. The buckling formulae in Eurocode 3 are based on second order moment and extensive experimentations on real columns.
2. Post-buckling analysis utilizing the Riks method in ABAQUS is an efficient way to evaluate the real effects of a column and gives the best convergence to test results.
3. The membrane residual stresses had a negligible influence on the section behavior and the bending component of residual stress has a larger influence on column buckling loads.
4. Mesh size influence buckling behavior.
5. Elastic-plastic with a strain hardening slope of E/100 gives a little higher buckling load but did not significantly affect the results and its effect reduce when the column heights increase.
6. Elastic-plastic without strain hardening is a little conservative approach as compared to other material behavior.
7. Residual stresses influence buckling behavior. However, the influence is reduced when the column heights and steel grade increases.
8. Rectangular sections have high buckling curve than that of square sections with the same slenderness ratio subjected to weak axis buckling. When the ratio height to width of a cross section (h/b) greater than 3, minor axis buckling curves gives "a_0"

for Steel Grade S355 to S460. The major axis buckling has the same buckling curves given in Eurocode 3.

5.2 Recommendations for Future Study

Throughout the chapters of this thesis some limitations were noted and are to be considered in a further continuation of this study:

1. The consideration of local effects in the hollow sections member is of major importance and as a result, a check shall be investigated on local effects in which the cross section resistance shall be reduced by the effective resistance.
2. More rectangular hollow section with different cross sections subjected to eccentric loads needs to be assessed to show the effect on Beam-Columns.
3. The effect of high strength steel needs to assessed to see the influence on flexural buckling curves.
4. For overall compressive behavior of hollow sections, it is desirable to perform FEM on the Cold-formed hollow sections additionally with the circular sections.

REFERENCES

1. Nseir, J., *Development of a New Design Method for the Cross-Section Capacity of Steel Hollow Sections,Ph.D. thesis*. Universite De Liege, 2015.

2. CEN, *EN10219-1: Cold-formed welded structural hollow sections of non-alloy and fine grain steels*. 2006, Brussels: European Committee for Standardization.

3. CEN, *EN10210-1: Hot finished structural hollow sections of non-alloy and fine grain structural steels Part 1. Part 1 Technical delivery conditions*. 2006, Brussels: European Committee for Standardization.

4. CEN, *EN10210-2: Hot finished structural hollow sections of non-alloy and fine grain structural steels Part 2. Part 2 Tolerances, dimensions and sectional properties*. 2006, Brussels: European Committee for Standardization.

5. *Celsius®355 NH technical guide Structural hollow sections*. Available from: https://www.tatasteelconstruction.com/en_GB/Products/structural-buildings-and-bridges/Structural-hollow-sections-hot-finished/Celsius%C2%AE-355.

6. ECCS, *Ultimate limit state calculation of sway frames with rigid joints.* ECCS Technical Committee 8 - structural stability: technical working group 8.2 - system, European Convention for Constructional Steelwork, , Publication No.33, 1984.

7. Key, P.W. and G.J. Hancock, *A theoretical investigation of the column behaviour of cold-formed square hollow sections.* Thin-Walled Structures, 1993. **16**(1–4): p. 31-64.

8. CEN, *Eurocode 3, EN-1993-1-1:2005, Eurocode 3: Design of steel structures*. 2005, Brussels: European Committee for Standardization

9. CEN, *Eurocode 3, EN-1993-1-5:2006, Eurocode 3: Plated structural elements*. 2006, Brussels: European Committee for Standardization.

10. *ESDEP (European Steel Design Education Programme). Columns.*; Available from: http://www.fgg.uni-lj.si~/pmoze/ESDEP/master/wg07/l0510.htm.

11. Boissonnade, N., et al., *Improvement of the interaction formulae for beam columns in Eurocode 3.* Computers & Structures, 2002. **80**(27): p. 2375-2385.

12. Dwight, J.B., *Use of Perry formula to represent the new European strut curves, IABSE reports of the working commissions = Rapports des commissions de travail AIPC = IVBH Berichte der Arbeitskommissionen.* 1975. **23**.

13. Dowling P.J., et al., *Eurocode no. 3: common unified rules for steel structures, Report EUR 8849 DE EN FR.* Commission of the European Communities, 1984.

14. Ellobody, E., R. Feng, and B. Young, *Finite Element Analysis and Design of Metal Structures*. 2014: Elsevier.

15. *ABAQUS CAE,v6.14,Simulia,2014*.

16. Schijve, J., *Fatigue of Structures and Materials*. 2009: Springer International Publishing.

17. Cruise, R.B. and L. Gardner, *Residual stress analysis of structural stainless steel sections.* Journal of Constructional Steel Research, 2008. **64**(3): p. 352-366.

18. Gardner, L., N. Saari, and F. Wang, *Comparative experimental study of hot-rolled and cold-formed rectangular hollow sections.* Thin-Walled Structures, 2010. **48**(7): p. 495-507.

19. Tong, L., et al., *Experimental investigation on longitudinal residual stresses for cold-formed thick-walled square hollow sections.* Journal of Constructional Steel Research, 2012. **73**: p. 105-116.

20. Zhang, X.-Z., et al., *Comparative experimental study of hot-formed, hot-finished and cold-formed rectangular hollow sections.* Case Studies in Structural Engineering, 2016. **6**: p. 115-129.

21. Somodi, B. and B. Kövesdi, *Residual stress measurements on cold-formed HSS hollow section columns.* Journal of Constructional Steel Research, 2017. **128**: p. 706-720.

22. CEN, *EN10020: Definition and classification of grades of steel*. 2000, Brussels: European Committee for Standardization.

APPENDIXES

Appendix A

Abaqus Input Files

Example input files used in the finite element modeling in ABAQUS are presented in this appendix. The SHS 203x203x6.3mm, with slenderness ratio L/r in of 95.7 input files presented are consistent with what is employed in the Numerical study. The first section, A1, is the Linear Buckling. The second section, A2, the Non Linear Buckling with membrane and bending residual stress.

Appendix A1

```
*Heading
** Job name: Linear_Buckling_Analysis22 Model name: Model-1
** Generated by: Abaqus/CAE 6.14-2
*Preprint, echo=NO, model=NO, history=NO, contact=NO
**
** PARTS
**
*Part, name=Part-1
*Node
 1, 0.0856999978, -0.0952000022, 7.63000011
 2, 0.0856999978, -0.101499997, 7.63000011
 3, 0.101499997, -0.0856999978, 7.63000011
 4, 0.0952000022, -0.0856999978, 7.63000011
 5, 0.0856999978, -0.101499997, 0.
 6, 0.101499997, -0.0856999978, 0.
 7, 0.0952000022, -0.0856999978, 0.
 8, 0.0856999978, -0.0952000022, 0.
 9, -0.0856999978, -0.0952000022, 7.63000011
 10, -0.0856999978, -0.0952000022, 0.
 11, -0.0856999978, -0.101499997, 0.
 12, -0.0856999978, -0.101499997, 7.63000011
 13, 0.0856999978, 0.101499997, 7.63000011
   .
   .
   .
   .
64162, 49171, 49172, 49180, 49179, 85779, 85780, 85788, 85787
64163, 49172, 49173, 49181, 49180, 85780, 85781, 85789, 85788
64164, 49173, 49174, 49182, 49181, 85781, 85782, 85790, 85789
64165, 49174, 49175, 49183, 49182, 85782, 85783, 85791, 85790
64166, 49175, 49176, 49184, 49183, 85783, 85784, 85792, 85791
64167, 49176, 3917, 3918, 49184, 85784, 21639, 21640, 85792
64168, 4316, 49177, 6345, 24, 25847, 85785, 49209, 5468
```

```
64169, 49177, 49178, 6346, 6345, 85785, 85786, 49210, 49209
64170, 49178, 49179, 6347, 6346, 85786, 85787, 49211, 49210
64171, 49179, 49180, 6348, 6347, 85787, 85788, 49212, 49211
64172, 49180, 49181, 6349, 6348, 85788, 85789, 49213, 49212
64173, 49181, 49182, 6350, 6349, 85789, 85790, 49214, 49213
64174, 49182, 49183, 6351, 6350, 85790, 85791, 49215, 49214
64175, 49183, 49184, 6352, 6351, 85791, 85792, 49216, 49215
64176, 49184, 3918, 19, 6352, 85792, 21640, 3920, 49216
*Nset, nset=_PickedSet2, internal, generate
 1, 85792, 1
*Elset, elset=_PickedSet2, internal, generate
 1, 64176, 1
** Section: Section-1
*Solid Section, elset=_PickedSet2, material=Material-1
,
*End Part
**
**
** ASSEMBLY
**
*Assembly, name=Assembly
**
*Instance, name=Part-1-1, part=Part-1
*End Instance
**
*Node
 1, 0., 0., 0.
*Node
 2, 0., 0., 7.63000011
*Nset, nset=_PickedSet8, internal
 1,
*Nset, nset=_PickedSet9, internal
 2,
*Nset, nset=_PickedSet10, internal
 2,
*Nset, nset=_PickedSet11, internal
 1,
*Nset, nset=_PickedSet13, internal
 2,
** Constraint: Constraint-1
*Rigid Body, ref node=_PickedSet8, pin nset=Part-1-1."Lower node"
** Constraint: Constraint-2
*Rigid Body, ref node=_PickedSet9, pin nset=Part-1-1."upper node"
*End Assembly
**
** MATERIALS
**
*Material, name=Material-1
*Density
7850.,
*Elastic
 2e+11, 0.3
** ----------------------------------------------------------------
```

```
**
** STEP: Linear Buckling
**
*Step, name="Linear Buckling", nlgeom=NO, perturbation
*Buckle
5, , 10, 1500
**
** BOUNDARY CONDITIONS
**
** Name: Bottom pinned Type: Displacement/Rotation
*Boundary, op=NEW, load case=1
_PickedSet11, 1, 1
_PickedSet11, 2, 2
_PickedSet11, 3, 3
_PickedSet11, 6, 6
*Boundary, op=NEW, load case=2
_PickedSet11, 1, 1
_PickedSet11, 2, 2
_PickedSet11, 3, 3
_PickedSet11, 6, 6
** Name: Top pinned Type: Displacement/Rotation
*Boundary, op=NEW, load case=1
_PickedSet10, 1, 1
_PickedSet10, 2, 2
*Boundary, op=NEW, load case=2
_PickedSet10, 1, 1
_PickedSet10, 2, 2
**
** LOADS
**
** Name: Load-1 Type: Concentrated force
*Cload
_PickedSet13, 3, -1.
**
** OUTPUT REQUESTS
**
*Restart, write, frequency=0
**
** FIELD OUTPUT: F-Output-1
**
*Output, field, variable=PRESELECT
*NODE FILE
U
*End Step
```

Appendix A2

```
*Heading
** Job name: NLBA1 Model name: Non-LBA
** Generated by: Abaqus/CAE 6.14-2
*Preprint, echo=NO, model=NO, history=NO, contact=NO
**
** PARTS
**
*Part, name=Part-1
*Node
 1, 0.0856999978, -0.0952000022, 7.63000011
 2, 0.0856999978, -0.101499997, 7.63000011
 3, 0.101499997, -0.0856999978, 7.63000011
 4, 0.0952000022, -0.0856999978, 7.63000011
 5, 0.0856999978, -0.101499997, 0.
 6, 0.101499997, -0.0856999978, 0.
 7, 0.0952000022, -0.0856999978, 0.
 8, 0.0856999978, -0.0952000022, 0.
 9, -0.0856999978, -0.0952000022, 7.63000011
 10, -0.0856999978, -0.0952000022, 0.
   .
   .
   .
   .
   .
64161, 49170, 49171, 49179, 49178, 85778, 85779, 85787, 85786
64162, 49171, 49172, 49180, 49179, 85779, 85780, 85788, 85787
64163, 49172, 49173, 49181, 49180, 85780, 85781, 85789, 85788
64164, 49173, 49174, 49182, 49181, 85781, 85782, 85790, 85789
64165, 49174, 49175, 49183, 49182, 85782, 85783, 85791, 85790
64166, 49175, 49176, 49184, 49183, 85783, 85784, 85792, 85791
64167, 49176, 3917, 3918, 49184, 85784, 21639, 21640, 85792
64168, 4316, 49177, 6345, 24, 25847, 85785, 49209, 5468
64169, 49177, 49178, 6346, 6345, 85785, 85786, 49210, 49209
64170, 49178, 49179, 6347, 6346, 85786, 85787, 49211, 49210
64171, 49179, 49180, 6348, 6347, 85787, 85788, 49212, 49211
64172, 49180, 49181, 6349, 6348, 85788, 85789, 49213, 49212
64173, 49181, 49182, 6350, 6349, 85789, 85790, 49214, 49213
64174, 49182, 49183, 6351, 6350, 85790, 85791, 49215, 49214
64175, 49183, 49184, 6352, 6351, 85791, 85792, 49216, 49215
64176, 49184, 3918, 19, 6352, 85792, 21640, 3920, 49216
                                        .
*Nset, nset=_PickedSet8, internal
 1,
*Nset, nset=_PickedSet9, internal
 2,
** Constraint: Constraint-1
```

```
*Rigid Body, ref node=_PickedSet8, pin nset=Part-1-1."Lower node"
** Constraint: Constraint-2
*Rigid Body, ref node=_PickedSet9, pin nset=Part-1-1."upper node"
*End Assembly
**
** MATERIALS
**
*Material, name=Material-1
*Density
7850.,
*Elastic
 2e+11, 0.3
*Plastic
 3.97e+08, 0.
**
** PREDEFINED FIELDS
**
** Name: A Type: Stress
*Initial Conditions, type=STRESS
A, 0., 0., -2.695e+07, 0., 0., 0.
** Name: B Type: Stress
*Initial Conditions, type=STRESS
B, 0., 0., -1.785e+07, 0., 0., 0.
** Name: C Type: Stress
*Initial Conditions, type=STRESS
C, 0., 0., -5.95e+06, 0., 0., 0.
** Name: D Type: Stress
*Initial Conditions, type=STRESS
D, 0., 0., 6.05e+06, 0., 0., 0.
** Name: E Type: Stress
*Initial Conditions, type=STRESS
E, 0., 0., 1.805e+07, 0., 0., 0.
** Name: F Type: Stress
*Initial Conditions, type=STRESS
F, 0., 0., 2.7e+07, 0., 0., 0.
** Name: inner Type: Stress
*Initial Conditions, type=STRESS
inner, 0., 0., -1.4e+08, 0., 0., 0.
** Name: outer Type: Stress
*Initial Conditions, type=STRESS
outer, 0., 0., 1.4e+08, 0., 0., 0.
** ----------------------------------------------------------------
**
** STEP: Non-Linear Buckling Analysis
**
*IMPERFECTION, FILE=Linear_Buckling_Analysis22, STEP=1
1,0.00763
*Step, name="Non-Linear Buckling Analysis", nlgeom=YES
*Static, riks
```

```
0.01, 1., 1e-45, 1., ,
**
** BOUNDARY CONDITIONS
**
** Name: BC-1 Type: Displacement/Rotation
*Boundary
Set-4, 1, 1
Set-4, 2, 2
** Name: BC-2 Type: Displacement/Rotation
*Boundary
Set-5, 1, 1
Set-5, 2, 2
Set-5, 3, 3
Set-5, 6, 6
**
** LOADS
**
** Name: Eigen Value Load Type: Concentrated force
*Cload
Set-3, 3, -1.02798e+06
**
** OUTPUT REQUESTS
**
*Restart, write, frequency=0
**
** FIELD OUTPUT: F-Output-1
**
*Output, field, variable=PRESELECT
**
** HISTORY OUTPUT: H-Output-1
**
*Output, history, variable=PRESELECT
*End Step
```

Appendix B

Appendix B summarizes the dimension of the hollow sections.

Section Dimensions and Properties - 203x203x6.3

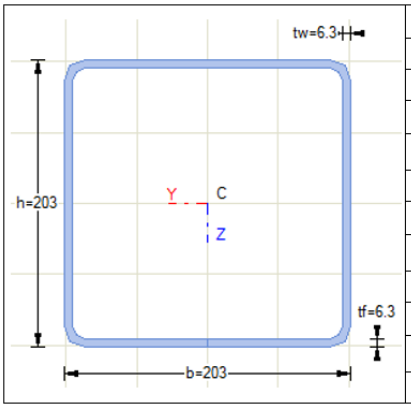

h [mm]	t_w [mm]	b [mm]	t_f [mm]		
203	6.3	203	6.3	203	6.3
r_i [mm]	r_o [mm]	A [cm^2]	A_{vz} [cm^2]	A_{vy} [cm^2]	
9.5	15.8	48.2	24.8	21.3	
I_y [cm^4]	I_z [cm^4]	$W_{el,y}$ [cm^3]	$W_{el,z}$ [cm^3]	$W_{pl,y}$ [cm^3]	$W_{pl,z}$ [cm^3]
3061.5	3061.5	301.6	301.6	352	352
i_y [cm]	i_z [cm]	C_z [cm]	C_y [cm]	I_t [cm^4]	W_t [cm^3]
8	8	10.2	10.2	4903.4	457.6

Section Dimensions and Properties - 340x100x10

Section Dimensions And Properties - 340x100x10 - RECTANGULAR TUBE

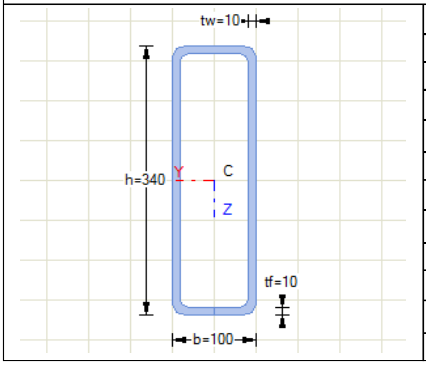

h [mm]	t_w [mm]	b [mm]	t_f [mm]		
340	10	100	10		
r_i [mm]	r_o [mm]	A [cm^2]	A_{vz} [cm^2]	A_{vy} [cm^2]	
10	15	82.9	64.1	18.8	
I_y [cm^4]	I_z [cm^4]	$W_{el,y}$ [cm^3]	$W_{el,z}$ [cm^3]	$W_{pl,y}$ [cm^3]	$W_{pl,z}$ [cm^3]
10585.1	1438.1	622.7	287.6	823.4	332.2
r_y [cm]	r_z [cm]	C_z [cm]	C_y [cm]	I_t [cm^4]	W_t [cm^3]
11.3	4.2	17	5	4299.1	521.3

Section Dimensions and Properties - 200x100x10

Section Dimensions And Properties - 200x100x10 - RECTANGULAR TUBE

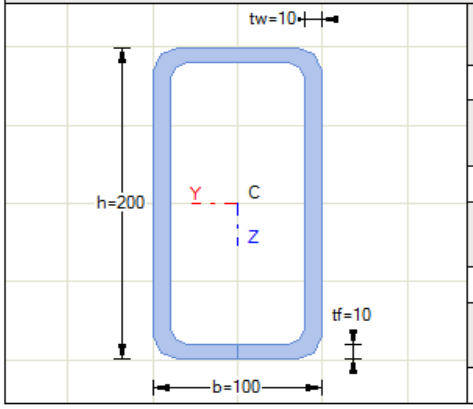

h [mm]	t_w [mm]	b [mm]	t_f [mm]		
200.0	10.0	100.0	10.0	100.0	10.0
r_i [mm]	r_o [mm]	A [cm^2]	A_{vz} [cm^2]	A_{vy} [cm^2]	
10.0	15.0	54.9	38.0	16.7	
I_y [cm^4]	I_z [cm^4]	$W_{el,y}$ [cm^3]	$W_{el,z}$ [cm^3]	$W_{pl,y}$ [cm^3]	$W_{pl,z}$ [cm^3]
2664.3	868.8	266.4	173.8	340.9	206.2
i_y [cm]	i_z [cm]	C_z [cm]	C_y [cm]	I_t [cm^4]	W_t [cm^3]
7.0	4.0	10.0	5.0	2161.9	294.7

Section Dimensions and Properties - 150x100x10

Section Dimensions And Properties - 150x100x10 - RECTANGULAR TUBE

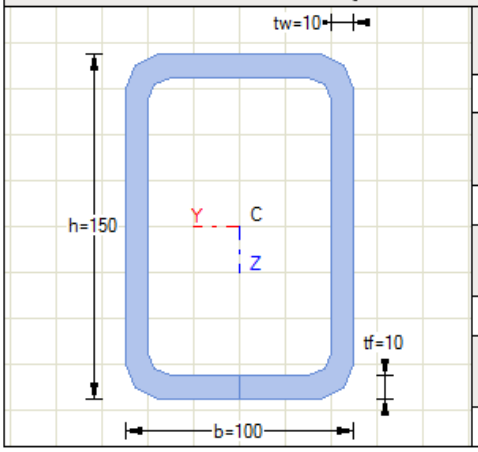

h [mm]	t_w [mm]	b [mm]	t_f [mm]		
150.0	10.0	100.0	10.0	100.0	10.0
r_i [mm]	r_o [mm]	A [cm^2]	A_{vz} [cm^2]	A_{vy} [cm^2]	
10.0	15.0	44.9	28.0	16.7	
I_y [cm^4]	I_z [cm^4]	$W_{el,y}$ [cm^3]	$W_{el,z}$ [cm^3]	$W_{pl,y}$ [cm^3]	$W_{pl,z}$ [cm^3]
1282.4	665.4	171.0	133.1	216.0	161.2
i_y [cm]	i_z [cm]	C_z [cm]	C_y [cm]	I_t [cm^4]	W_t [cm^3]
5.3	3.8	7.5	5.0	1439.0	213.9

Section Dimensions and Properties - 100x100x10

Section Dimensions And Properties - 100x10 - RECTANGULAR TUBE

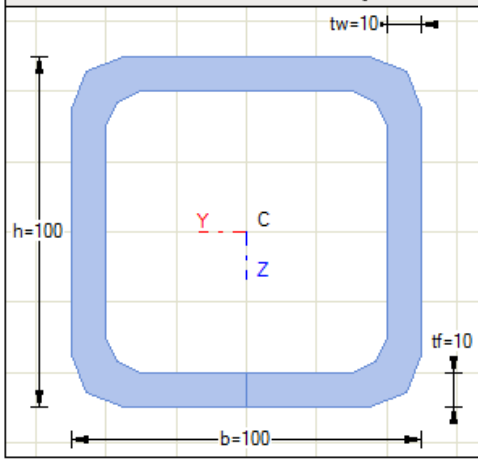

h [mm]	t_w [mm]	b [mm]	t_f [mm]		
100.0	10.0	100.0	10.0	100.0	10.0
r_i [mm]	r_o [mm]	A [cm^2]	A_{vz} [cm^2]	A_{vy} [cm^2]	
10.0	15.0	34.9	18.0	16.7	
I_y [cm^4]	I_z [cm^4]	$W_{el,y}$ [cm^3]	$W_{el,z}$ [cm^3]	$W_{pl,y}$ [cm^3]	$W_{pl,z}$ [cm^3]
462.1	462.1	92.4	92.4	116.2	116.2
i_y [cm]	i_z [cm]	C_z [cm]	C_y [cm]	I_t [cm^4]	W_t [cm^3]
3.6	3.6	5.0	5.0	767.7	133.2